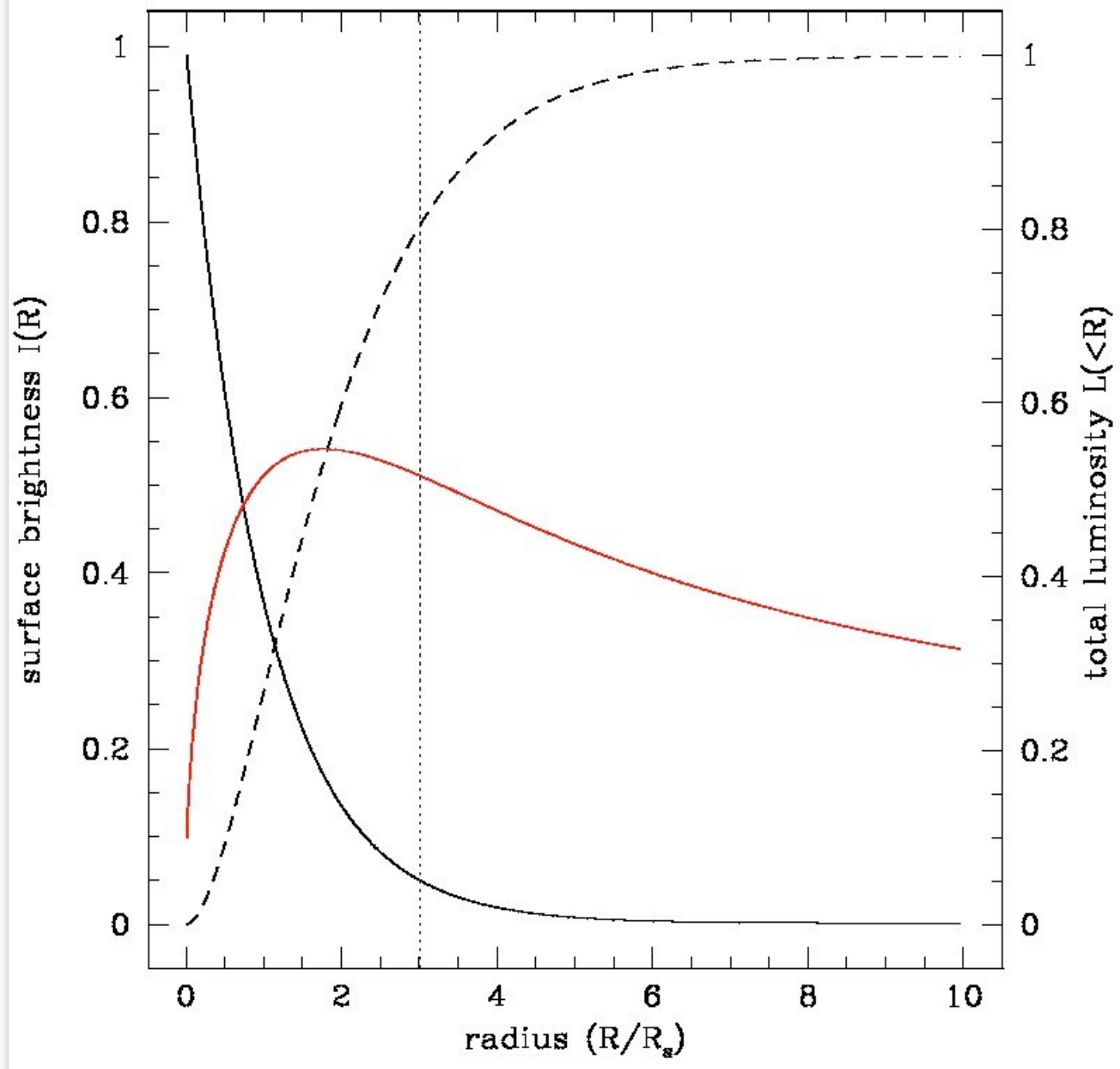
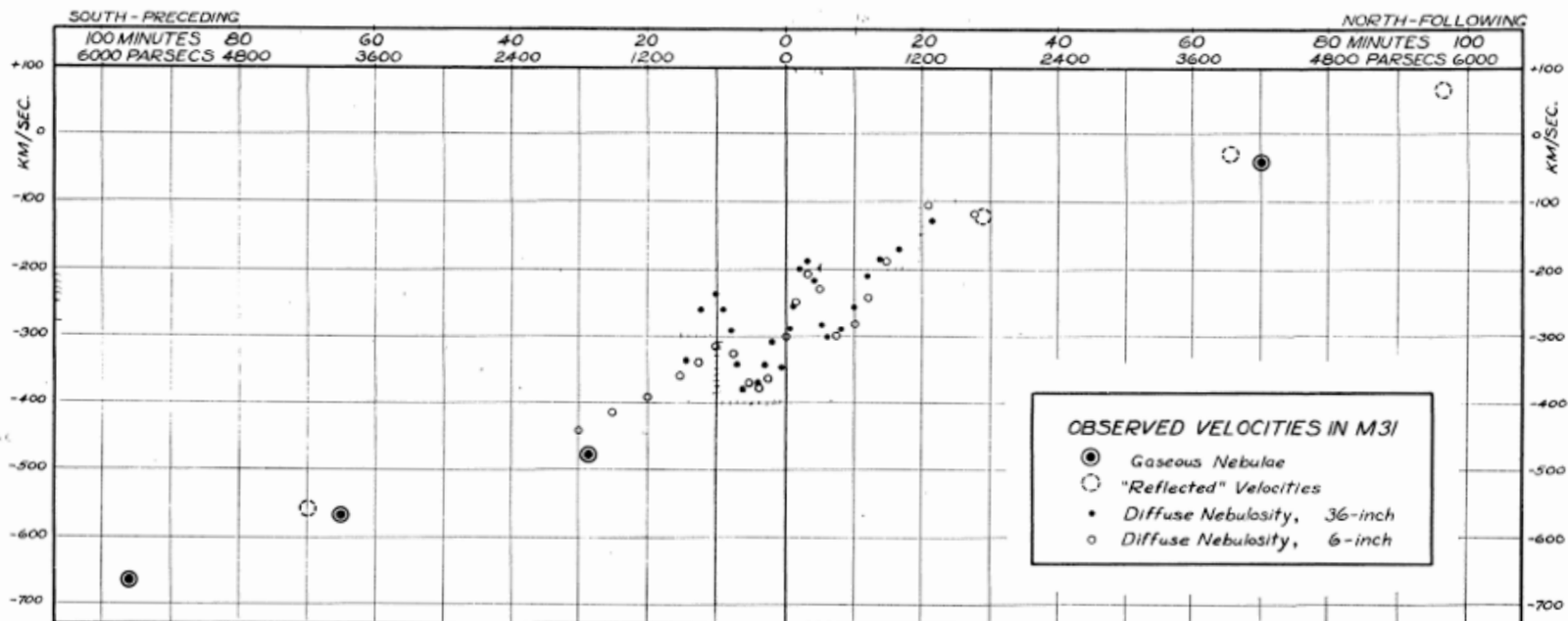
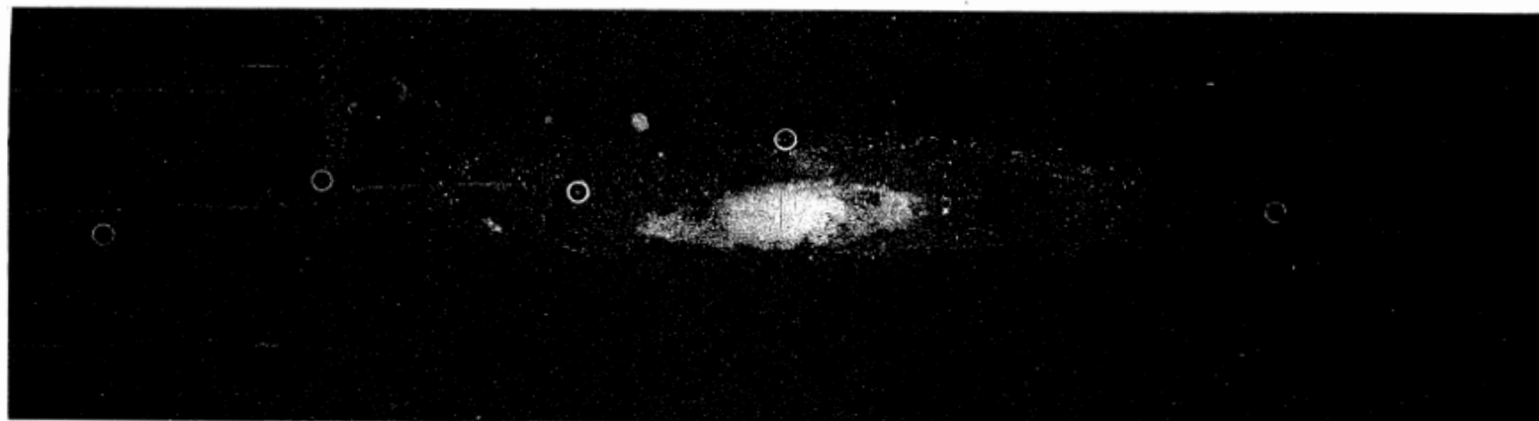


5. Dark matter





The Andromeda Nebula, with observed velocities plotted below. Smoothed mean velocities of the unresolved central portion are represented by small dots for observations with the Crossley reflector, and by small open circles for observations with the 6-inch mirror. In the photograph, the bright-line emission nebulosities are encircled, and their velocities, with the exception of the one on the minor axis, are plotted as ringed dots. (Photograph by Mayall)

III. THE ROTATIONAL VELOCITIES, $R > 16'$ (3.2 KPC)

For an emission region with nebular coordinates R, θ , the observed radial velocity is related to the circular-velocity component $V(R)$ and the expansion component $E(R)$ through the equation

$$V_{\text{obs}} - V_e = V(R) \sin \xi \cos \theta + E(R) \sin \xi \sin \theta, \quad (1)$$

where V_e is the systemic velocity of the galaxy. In terms of the observed coordinates X, Y , $\cos \theta = X/R$, $\sin \theta = (Y \sec \xi)/R$, $R = (X^2 + Y^2 \sec^2 \xi)^{1/2}$. The angle ξ is the angle between the line of sight and the perpendicular to the plane of the galaxy. For M31, a value of 77° for ξ is adopted because it is the mean of several optical determinations, and also because it was used by Burke, Turner, and Tuve (1964) and by Roberts (1966) and hence allows a direct comparison of the optical results with the 21-cm observations. A more detailed discussion of the geometrical parameters for M31 can be found

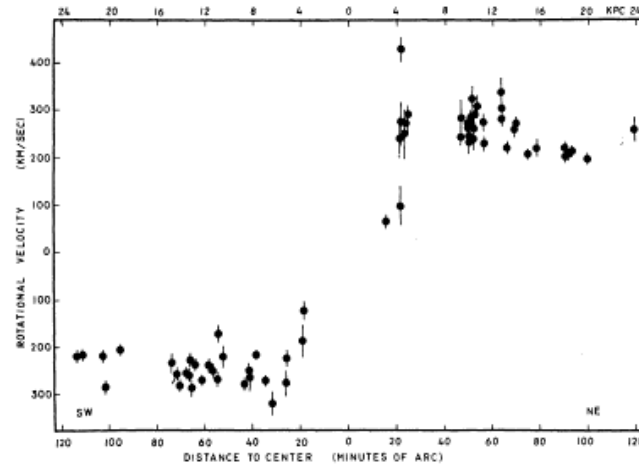
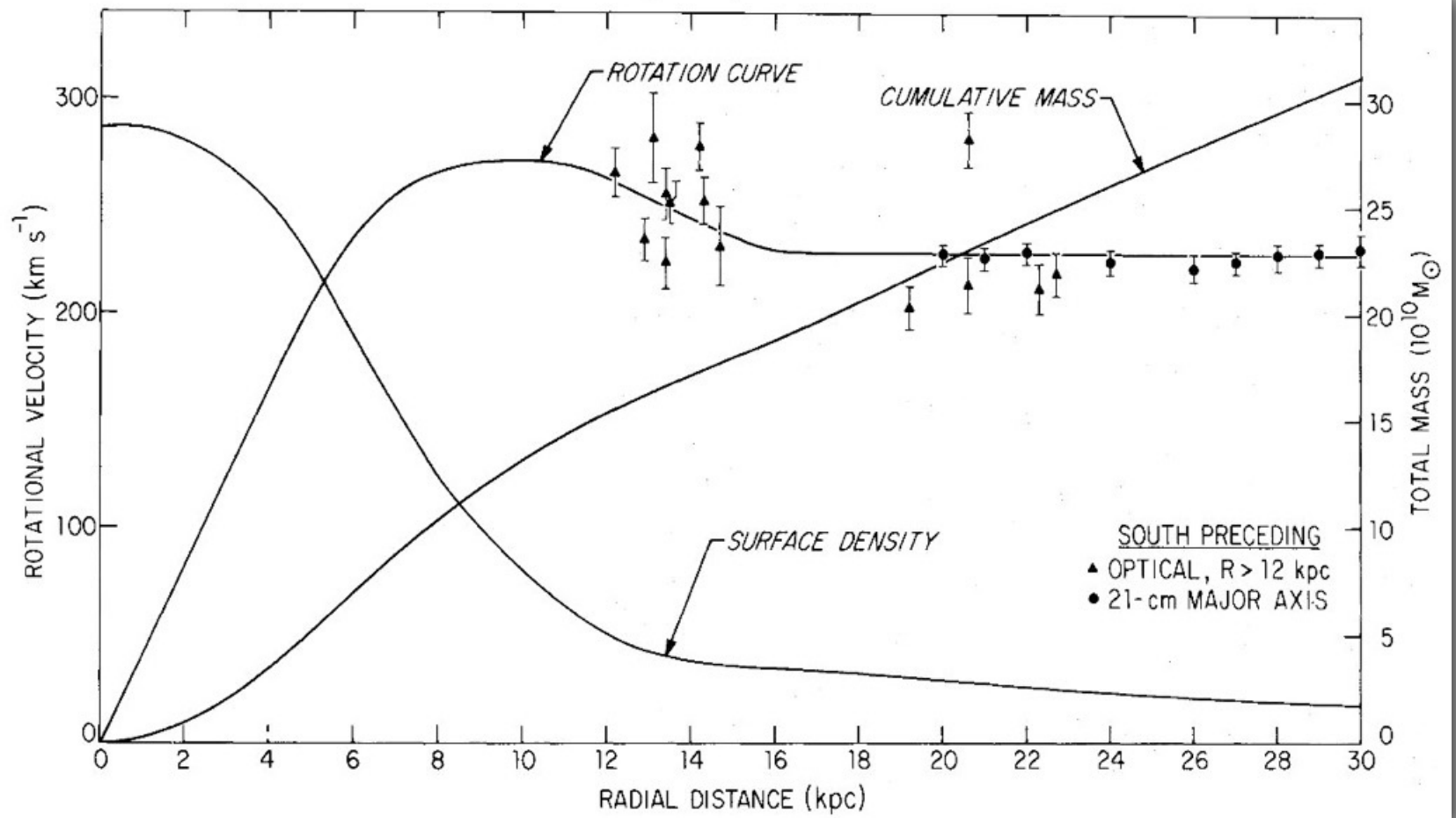


FIG. 3.—Rotational velocities for sixty-seven emission regions in M31, as a function of distance from the center. Error bars indicate average error of rotational velocities.

elsewhere (Rubin and D'Odorico 1969). The position angle of the major axis is taken as 38° . From symmetry considerations, and because it is near the mean value $V_e = -302$ observed from the $[N \text{ II}] \lambda 6583$ emission line at the nucleus, V_e is taken as -300 km sec^{-1} . The remaining assumption in equation (1) is that all motions are constrained to the principal plane of M31. If expansion motions are not present, $E(R) = 0$, and the second term in equation (1) vanishes. Hence, we can determine a circular velocity from the observed radial velocity of each emission region from the relation

$$V_{\text{obs}} + 300 = V(R) \sin 77^\circ (X/R). \quad (2)$$

The calculated circular velocities are listed in column (8) of Table 1, along with the error of the circular velocities. Errors have been formed from the average errors of the radial velocities, increased by the projection factor $p = \csc 77^\circ \sec \theta$. For regions along the major axis, $p = 1.026$; for regions with $\theta = 45^\circ$, $p = 1.45$. In Figure 3 the circular velocities for all sixty-seven emission regions are plotted as a function of distance from the center. The velocities increase rapidly in the region $3.2 < R < 5.0 \text{ kpc}$, and decrease slowly in the outer regions of the galaxy.



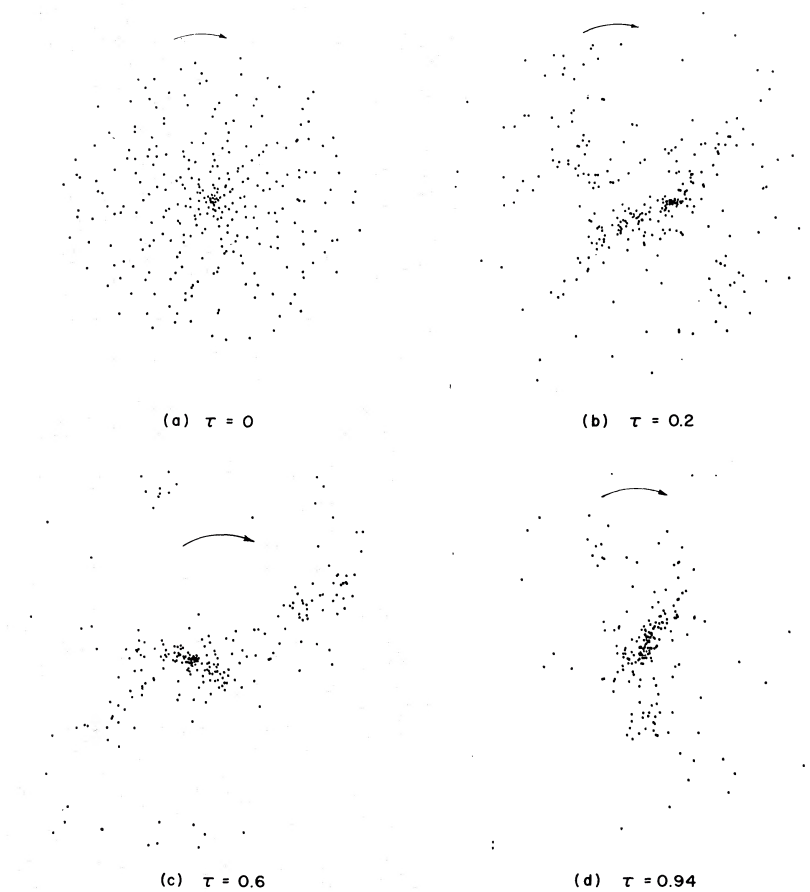


FIG. 4.—Evolution of model 1. The graphs show the positions of the mass points projected onto the plane, at four instants.

relaxation processes for individual particles, whether due to numerical error or to two-body collisions. We may expect, therefore, that a given numerical error may be less serious here than in some other applications of N -body models.

2. We have rounded over the potential at small distance, thereby making the mathematical problem nonsingular and removing the largest fluctuations in acceleration from the computational problem.

3. We judge from trial applications of the integration scheme, where the analytic solution is known, that the time step should be small enough for the integration to carry one particle past another one reliably (but not with great accuracy) whatever the impact parameter for expected particle relative velocities.

Research Note

Comparison of Rotation Curves of Different Galaxy Types

M. S. Roberts* and A. H. Rots

Kapteyn Astronomical Institute, University of Groningen

Received November 23, 1972, revised April 13, 1973

Summary. Rotation curves extending to large radial distances are now available for 3 spiral galaxies, each of a different type. Differences in shape of the rotation curves indicate a mass distribution that is related to structural type and is in the same sense as the luminosity distribution for these galaxies. The shapes of the

rotation curves at large radii indicate a significant amount of matter at these large distances and imply that spiral galaxies are larger than found from photometric measurements.

Key words: galaxies – rotation curves

The rotation curve of a galaxy is determined mainly by the balance between the system's centrifugal and gravitational forces. The mass distribution giving rise to the gravitational forces is thus reflected in the rotation curve and may be evaluated from such curves. The procedures and assumptions are extensively discussed in the literature, e.g. Brandt (1960), Perek (1962), Prendergast (1962), Toomre (1963).

The extent over which the mass distribution may be described is directly related to the radial extent over which the rotation curve has been determined. Observational constraints have, unfortunately, limited most rotation curves to a small fraction (typically 1/3 to 1/2) of the optically measured radius.

Rotation curves which do extend to large distances are now available for M 101 (Rogstad and Shostak, 1972), M 31 (Rubin and Ford, 1970; Roberts and Whitehurst, 1972), and M 81 (this paper). This sample of spiral galaxies is particularly fortunate since each is representative of a different structural type: Scd, Sb, and Sab, respectively, while the total mass for each system, as derived by the above authors, is $2 \times 10^{11} M_{\odot}$ to within a factor of ~ 2 .

The rotation curves for these systems are shown in Fig. 1. Each is a smoothed curve of the actual data. For M 81 the curve within 18 kpc is from unpublished results using the Westerbork Synthesis Radio Telescope¹⁾ with a resolution of $\sim 50''$. The outer extension is based on 300-foot data ($10'$ beam) obtained at the National Radio Astronomy Observatory. These data

* On leave from the National Radio Astronomy Observatory, which is operated by Associated Universities, Inc., under contract with the National Science Foundation.

¹⁾ The Westerbork Radio Observatory is operated by the Netherlands Foundation for Radio Astronomy with the financial support of the Netherlands Organization for the Advancement of Pure Research (Z.W.O.).

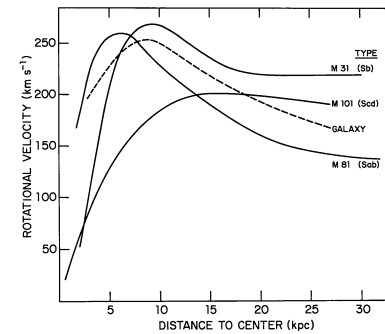


Fig. 1. Rotation curves for the galaxies M 31, M 101, and M 81 are shown as solid lines. The rotation curve for our galaxy is included for comparative purposes only. It is shown as a dashed line

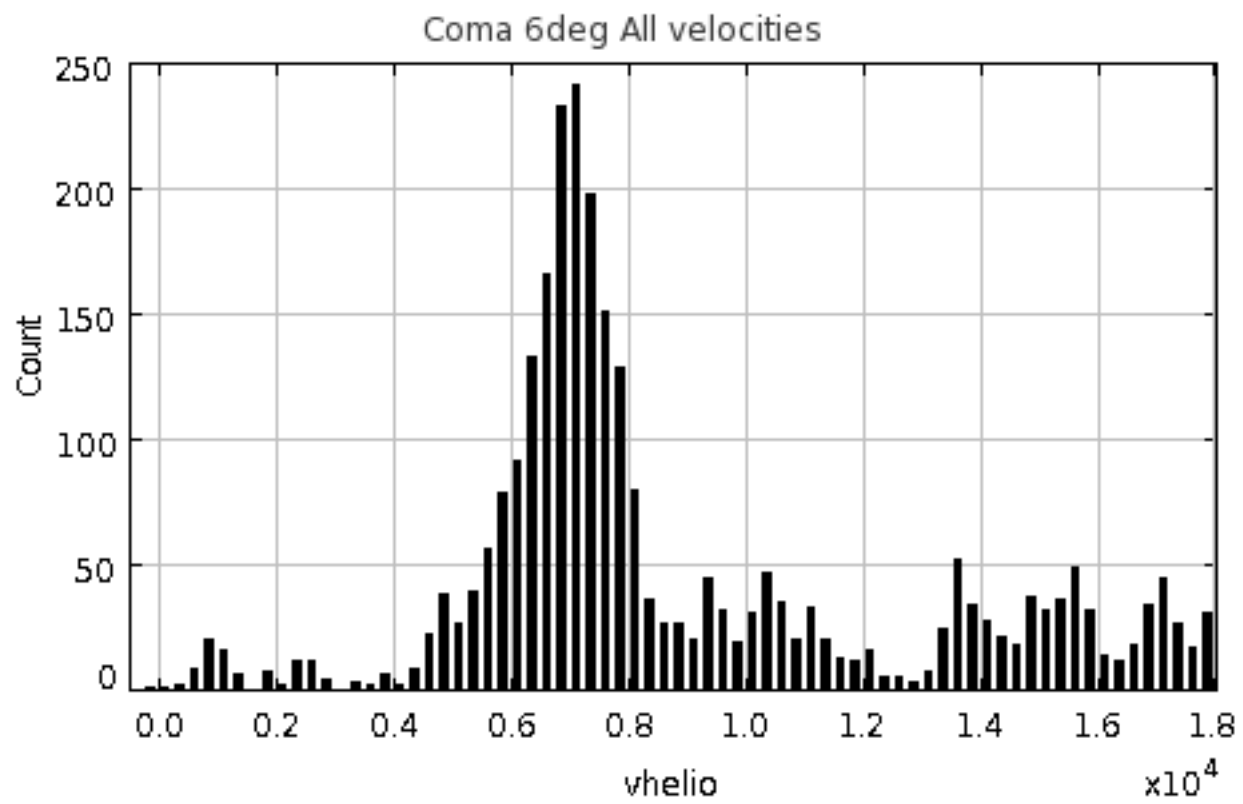
confirm and extend Munch's (1959) earlier optical measurements. The M 31 rotation curve to ~ 24 kpc is from the optical study by Rubin and Ford (1970). The region of constant rotational velocity they observe in the outermost 4 kpc is also found in 21-cm observations

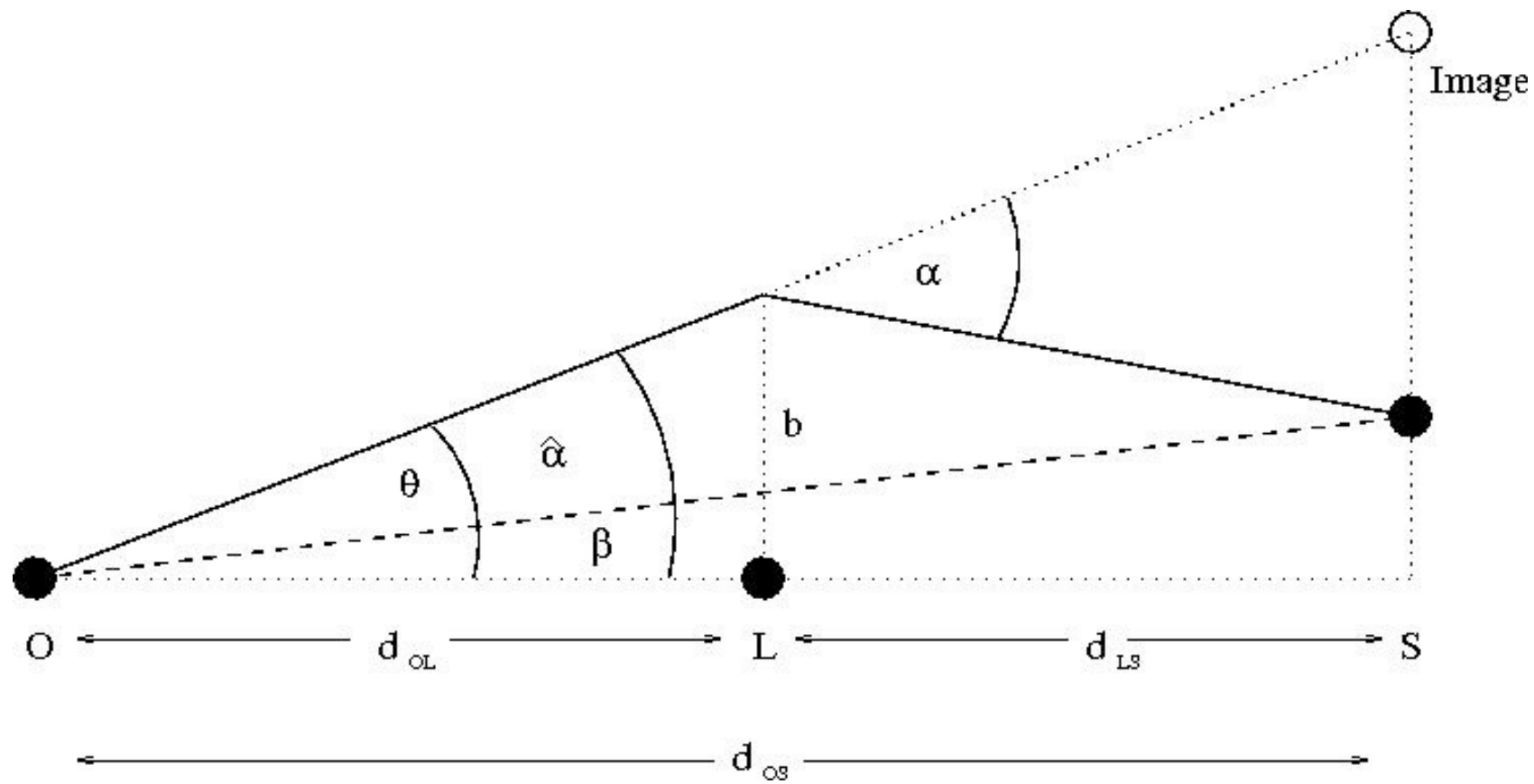
Table 1. Properties of galaxies

Galaxy	Type	Distance (Mpc)	Incl. (°)	Semi major axis* (kpc)	Rot. curve limiting radius (kpc)
M 31	Sb	0.69	77	19.8	29.0
M 81	Sab	3.25	55	16.5	31.0
M 101	Scd	6.9	22	28.1	26.5
Galaxy	(Sbc)	—	—	—	—

* Measured to a surface magnitude of $26^m.5$ per square arc second. E. Holmberg, *Medd. Lund.*, Series II, No. 136, 1958.







Magnification

Gravitational lensing preserves surface brightness, but changes the apparent solid angle of the source => magnification

$$\text{magnification} = \frac{\text{image area}}{\text{source area}}$$

Magnification calculated using the lens equation as

$$\mu = \left| \det \left(\frac{\partial \beta}{\partial \theta} \right) \right|^{-1} \equiv \left| \det \left(\frac{\partial \beta_i}{\partial \theta_j} \right) \right|^{-1} \quad \text{If circularly symmetric} \quad \mu = \frac{\theta}{\beta} \frac{d\theta}{d\beta}$$

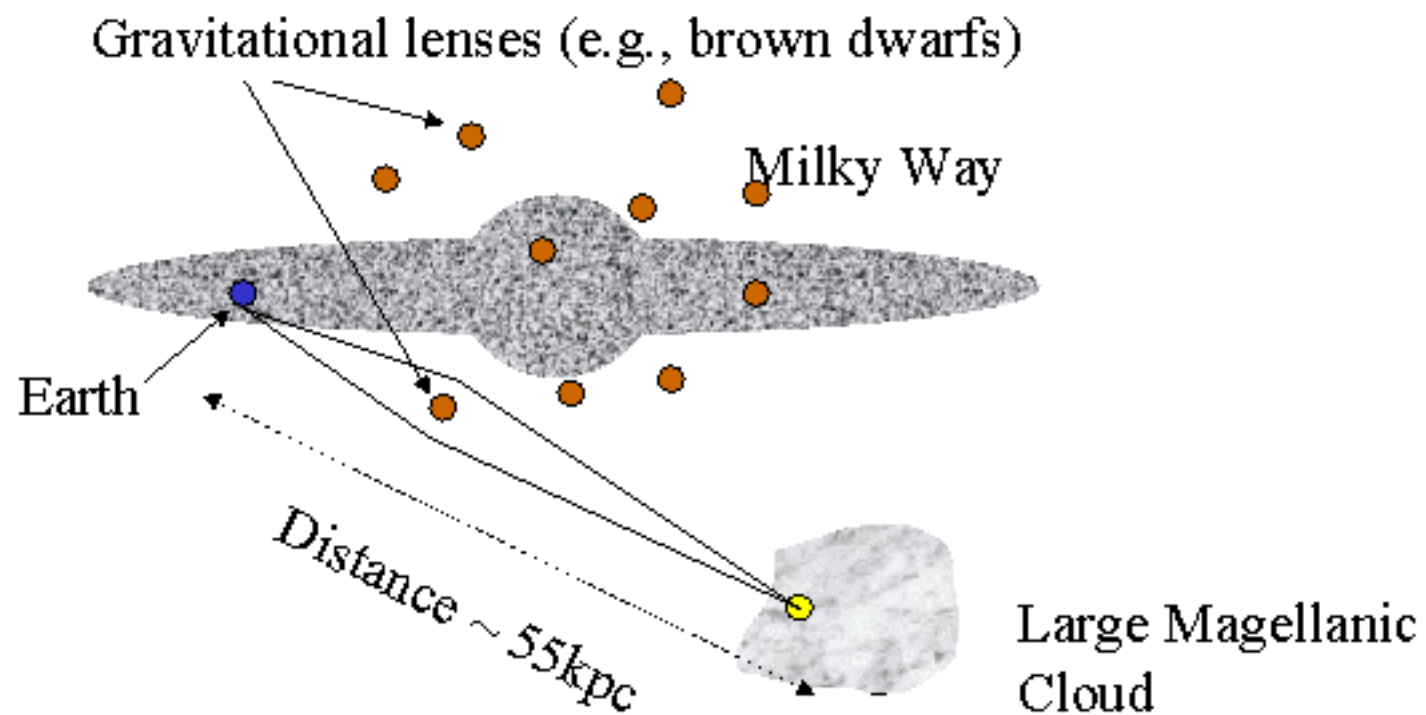
Example: point mass

Images $\theta_{\pm} = \frac{1}{2} \left(\beta \pm \sqrt{\beta^2 + 4\theta_E^2} \right)$ $u = \beta\theta_E^{-1}$.

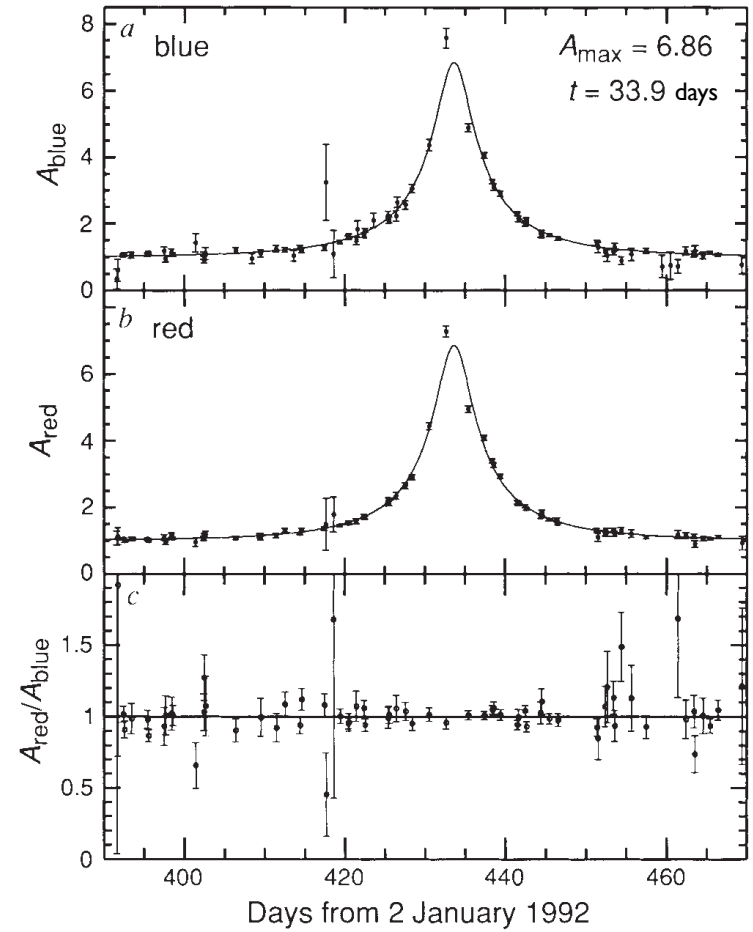
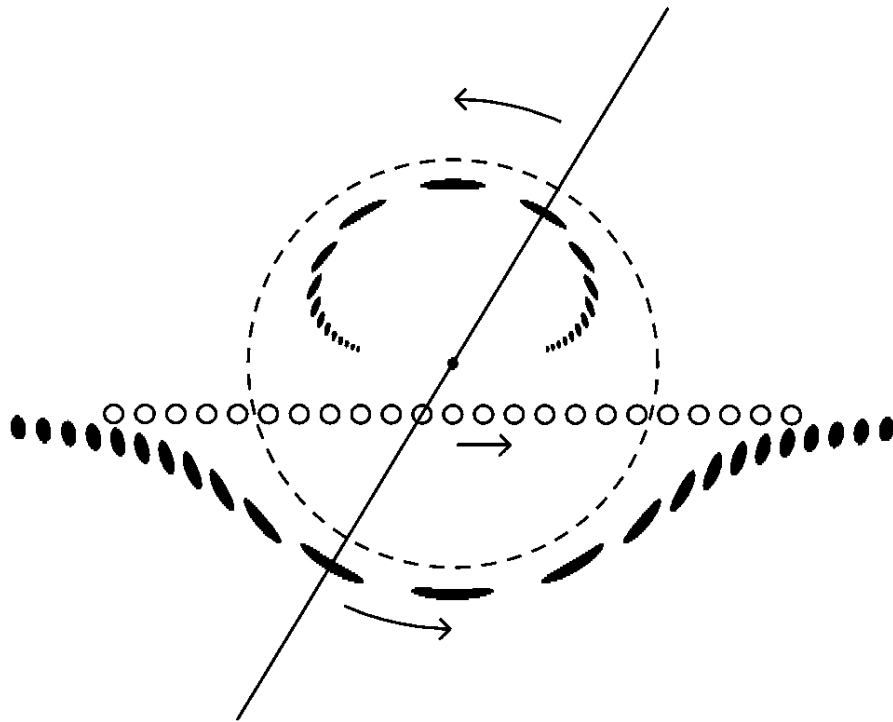
magnification $\mu_{\pm} = \left[1 - \left(\frac{\theta_E}{\theta_{\pm}} \right)^4 \right]^{-1} = \frac{u^2 + 2}{2u\sqrt{u^2 + 4}} \pm \frac{1}{2}$
 + image always magnified
 - image can go either way

total magnification $\mu = |\mu_+| + |\mu_-| = \frac{u^2 + 2}{u\sqrt{u^2 + 4}}$

Source on Einstein ring $\beta = \theta_E, u = 1$ $\mu = 1.17 + 0.17 = 1.34$

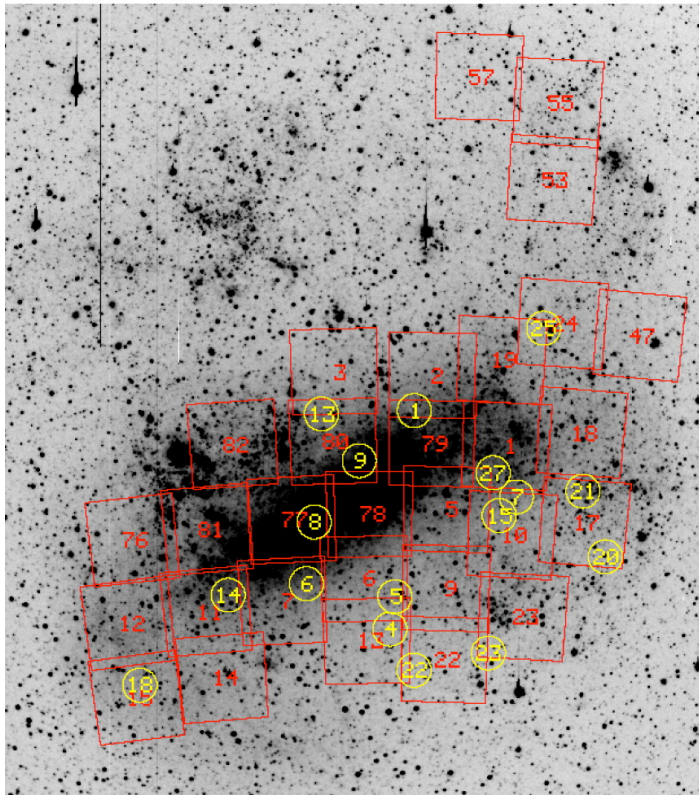


Microlensing



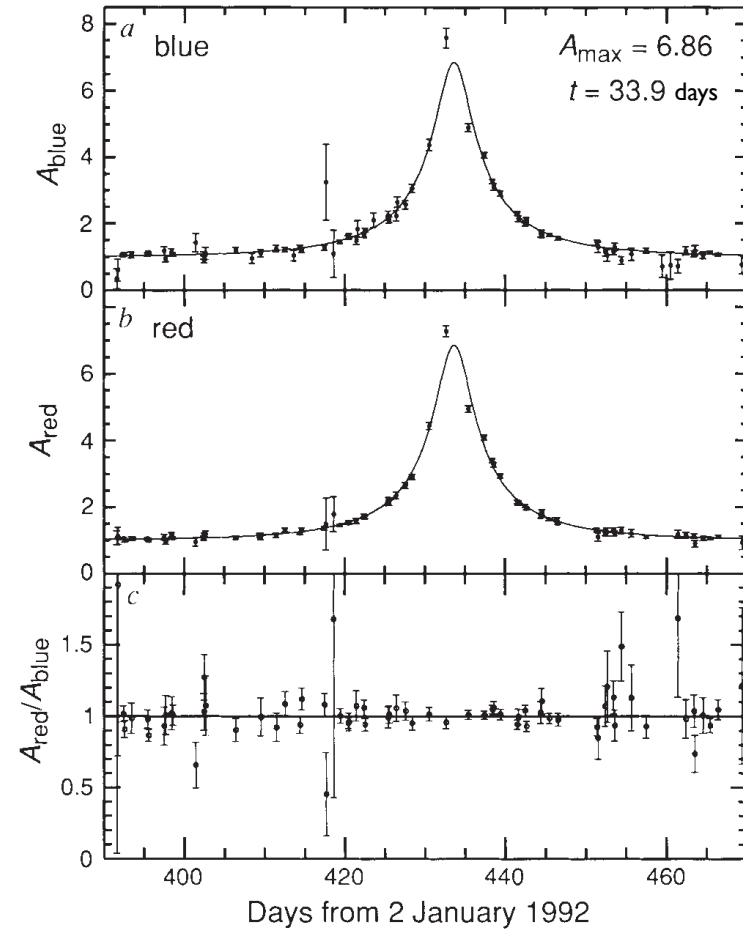
Microlensing requirements

17 microlensing events towards LMC
after ~5.7 years watching 11.9 million stars



Alcock et al (1993,2000)
MACHO collaboration

Same lightcurve seen in two wavelength
bands - used to exclude variable stars



$$t \sim 100 \sqrt{M_{\text{macho}} / M_{\odot}} \text{ days}$$

$t = 33.9$ days



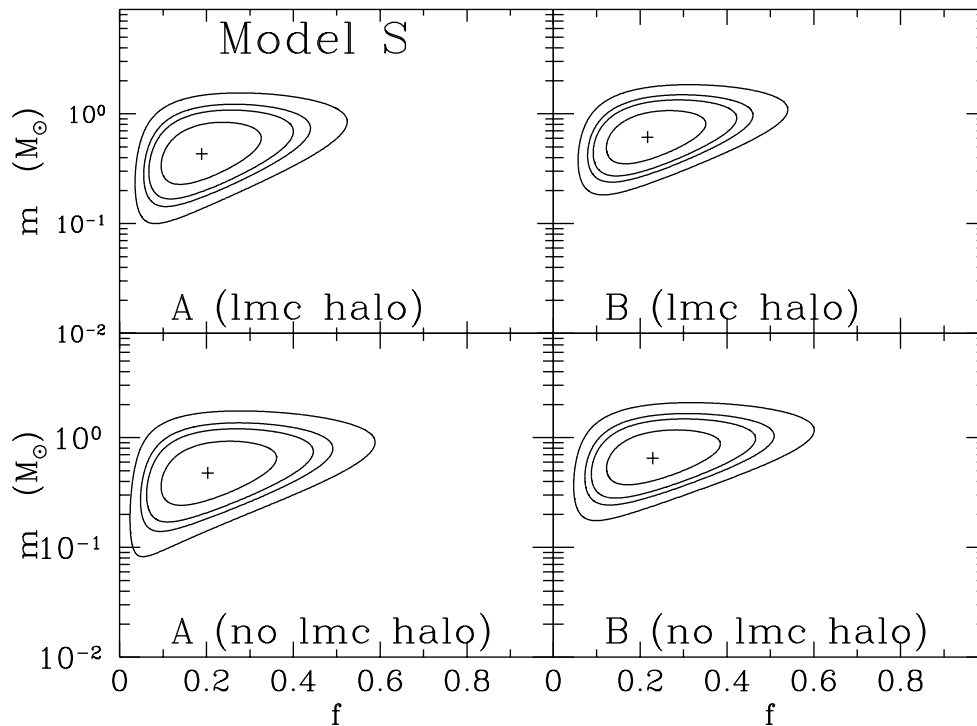
$M \sim 0.12 M_{\text{sol}}$

Observations: MACHO survey

17 microlensing events towards LMC
after ~5.7 years watching 11.9 million stars

$$\longrightarrow \tau_2^{400} = 1.2_{-0.3}^{+0.4} \times 10^{-7}$$

Larger than expected if no MACHOs...



What is the dark matter?

MACHO=Massive Compact Halo Object

WIMP = Weakly Interacting Massive Particle

MACHO constraint is wierd. Suggests
~0.2 galaxy mass in ~0.5 Msol objects.
Hard to explain...

Too light to be white dwarves, neutron stars.

Alcock et al. 2000
(MACHO collaboration)

Zwicky's leap

- Although calculations of lensing by other stars were carried out the small angular separations of the images led to pessimism that they could be seen
- In 1937, Zwicky made the jump of suggesting that extragalactic nebulae (galaxies) would produce well separated images that could be observed
 - by applying the virial theorem to the Coma and Virgo clusters he was (correctly) using masses ~ 400 times larger than was then believed
- He pointed out that gravitational lensing would allow the study of objects at greater distances (via magnification), that many arcs should be visible, and the importance of magnification bias in magnitude limited samples.

Zwicky 1937

Nebulae as Gravitational Lenses

The discovery of images of nebulae which are formed through the gravitational fields of nearby nebulae would be of considerable interest for a number of reasons.

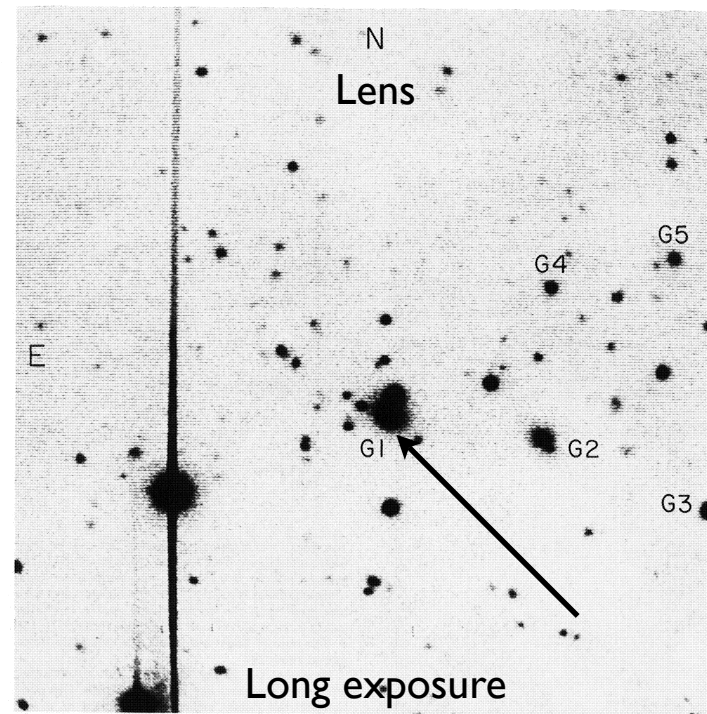
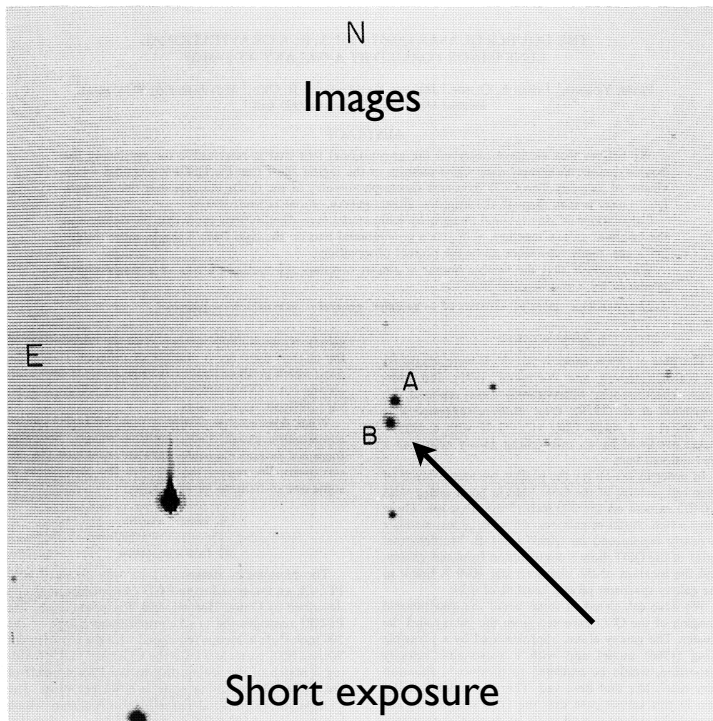
(1) It would furnish an additional test for the general theory of relativity.

(2) It would enable us to see nebulae at distances greater than those ordinarily reached by even the greatest telescopes. Any such *extension* of the known parts of the universe promises to throw very welcome new light on a number of cosmological problems.

(3) The problem of determining nebular masses at present has arrived at a stalemate. The mass of an average nebula until recently was thought to be of the order of $M_N = 10^9 M_\odot$, where M_\odot is the mass of the sun. This estimate is based on certain deductions drawn from data on the intrinsic brightness of nebulae as well as their spectrographic rotations. Some time ago, however, I showed² that a straightforward application of the virial theorem to the great cluster of nebulae in Coma leads to an average nebular mass four hundred times greater than the one mentioned, that is, $M_N' = 4 \times 10^{11} M_\odot$. This result has recently been verified by an investigation of the Virgo cluster.³ Observations on the deflection of light around nebulae may provide the most direct determination of nebular masses and clear up the above-mentioned discrepancy.

Discovery of 0957+56 I

- The first concrete example of a gravitational lens was reported in 1979 in the form of the quasar QSO 957+56 I A,B found at $z \sim 1.4$ (Walsh, Carswell & Weymann 1979). Two seen images separated by 6".
- Evidence that this is a lens comes from
 1. Lensing galaxy detected at $z \sim 0.36$
 2. Similarity of the spectra of the two images
 3. Ratio of optical and radio fluxes are consistent between two images
 4. VLBI imaging showed detailed correspondence between small scale features



Images of QSO 0957+561

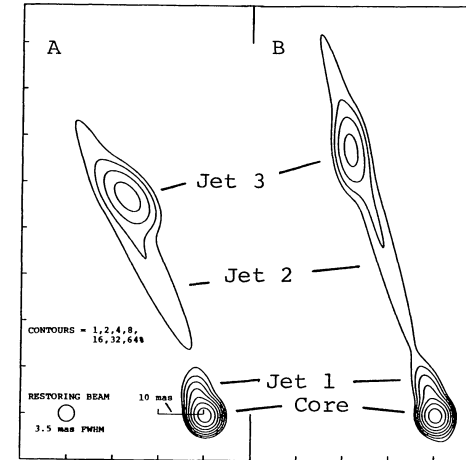
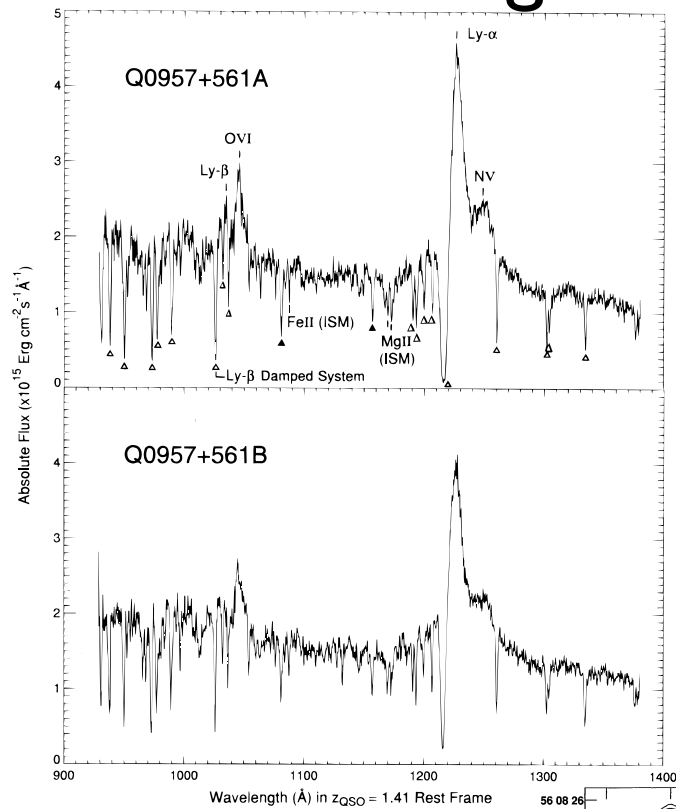
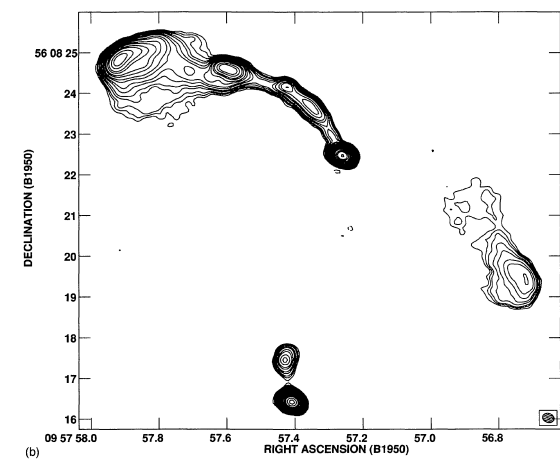
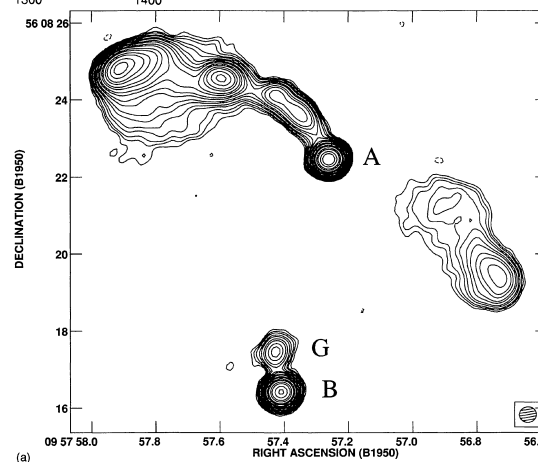


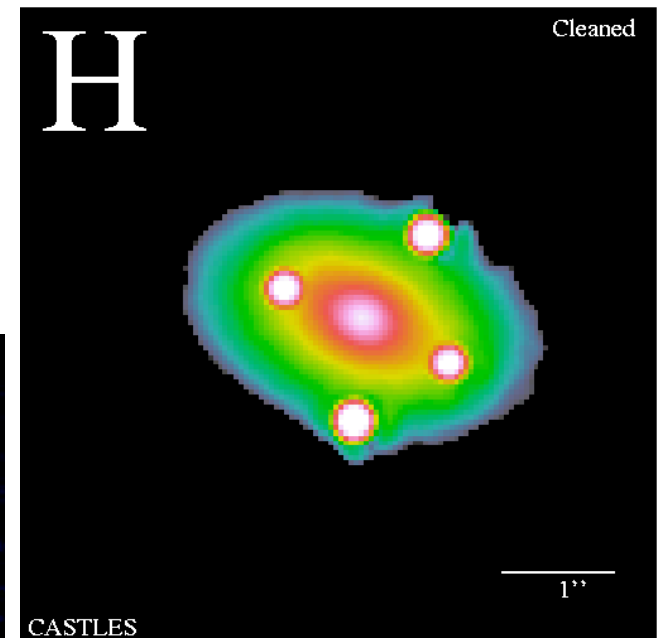
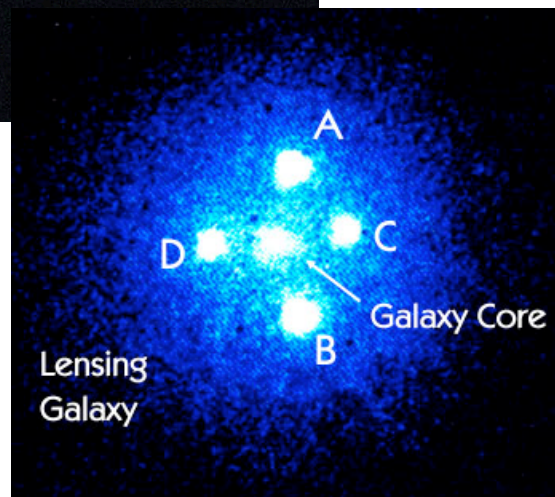
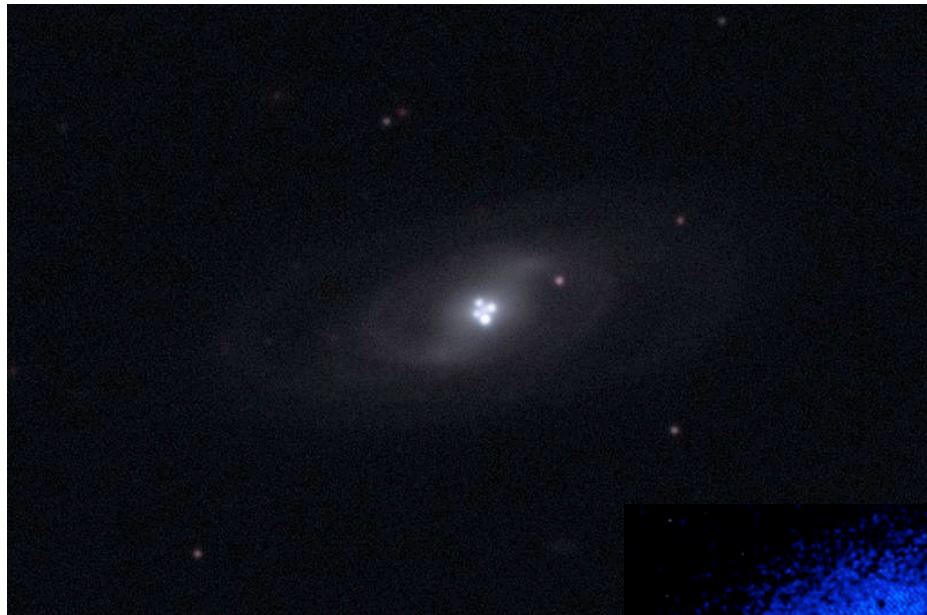
Figure 1 — The brightness distributions of 0957+561A and B. Four elliptical Gaussian components account for the data obtained from the 1981 $\lambda 13$ cm VLBI observations for A and for B (Model I—see text). The correspondences in the number and in the properties of the components of the respective models, and the evidence for a change in parity from one image to the other, all support the hypothesis that A and B are images of a single object.



“Huchra’s Lens”

- Quadruply-imaged quasar Q2237+0305 “Einstein Cross” $z=1.7$ with image separation $\sim 1.8''$ \rightarrow elliptical lens
- Lensing galaxy is ZW2237+030 “Huchra’s Lens” at $z=0.04$

Huchra+(1985)



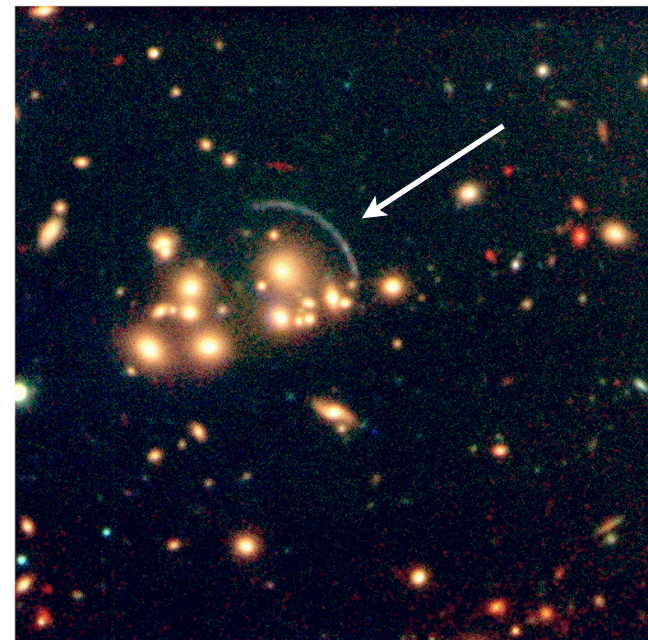
Nearby and isolated
 \rightarrow key system for testing GR

Cluster Arcs

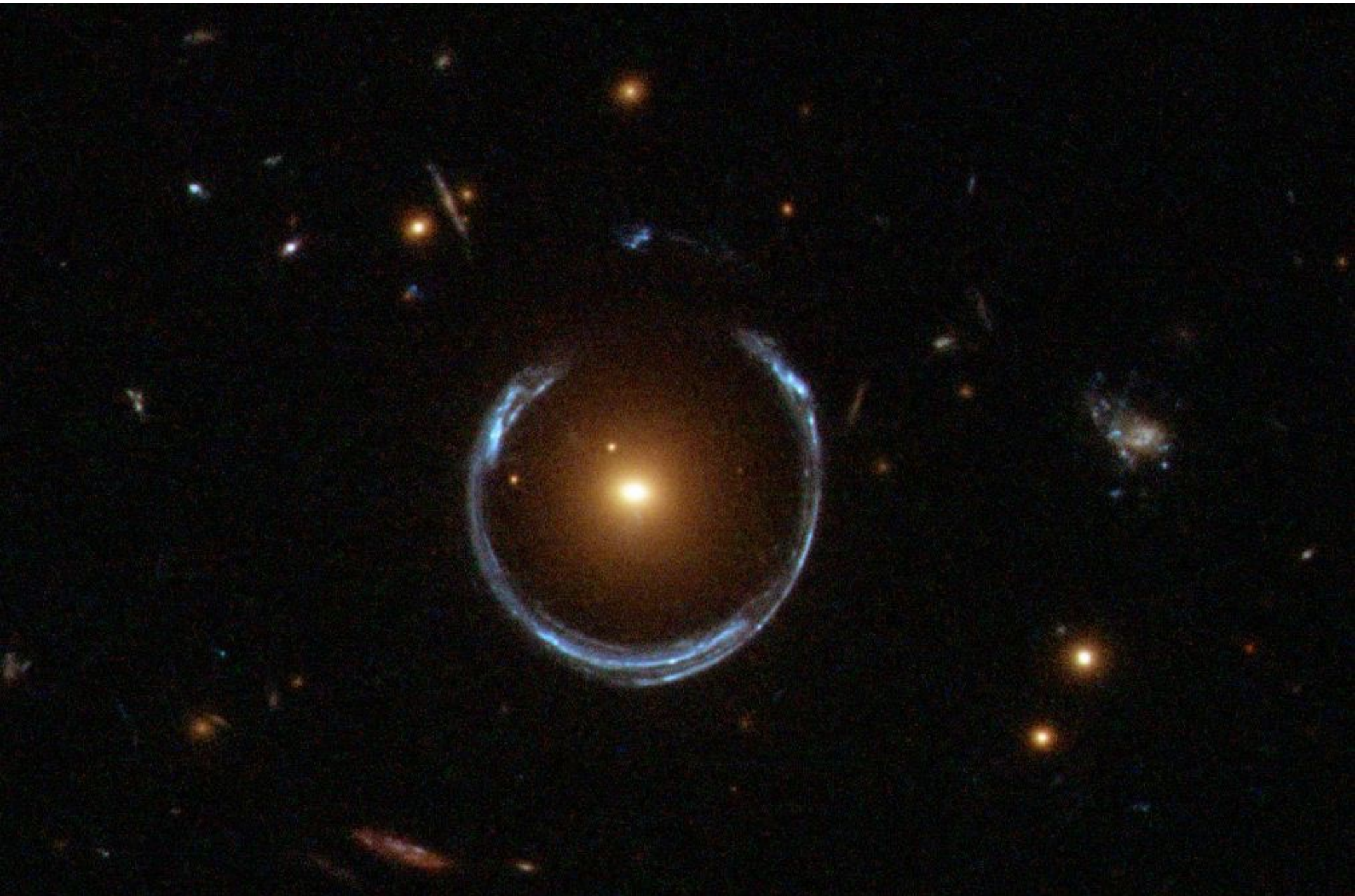
- In 1986, two groups discovered stretched arcs in clusters of galaxies at high redshift. “giant luminous arcs” - very thin in radial direction (unresolved)
- Light from arc confirmed to be from a much higher redshift source
- Confounded expectations based on pre-ROSAT X-ray observations that the surface mass density of clusters was too low to cause strong lensing
- Suddenly everyone found arcs in their old data...



Abel 370 - HST

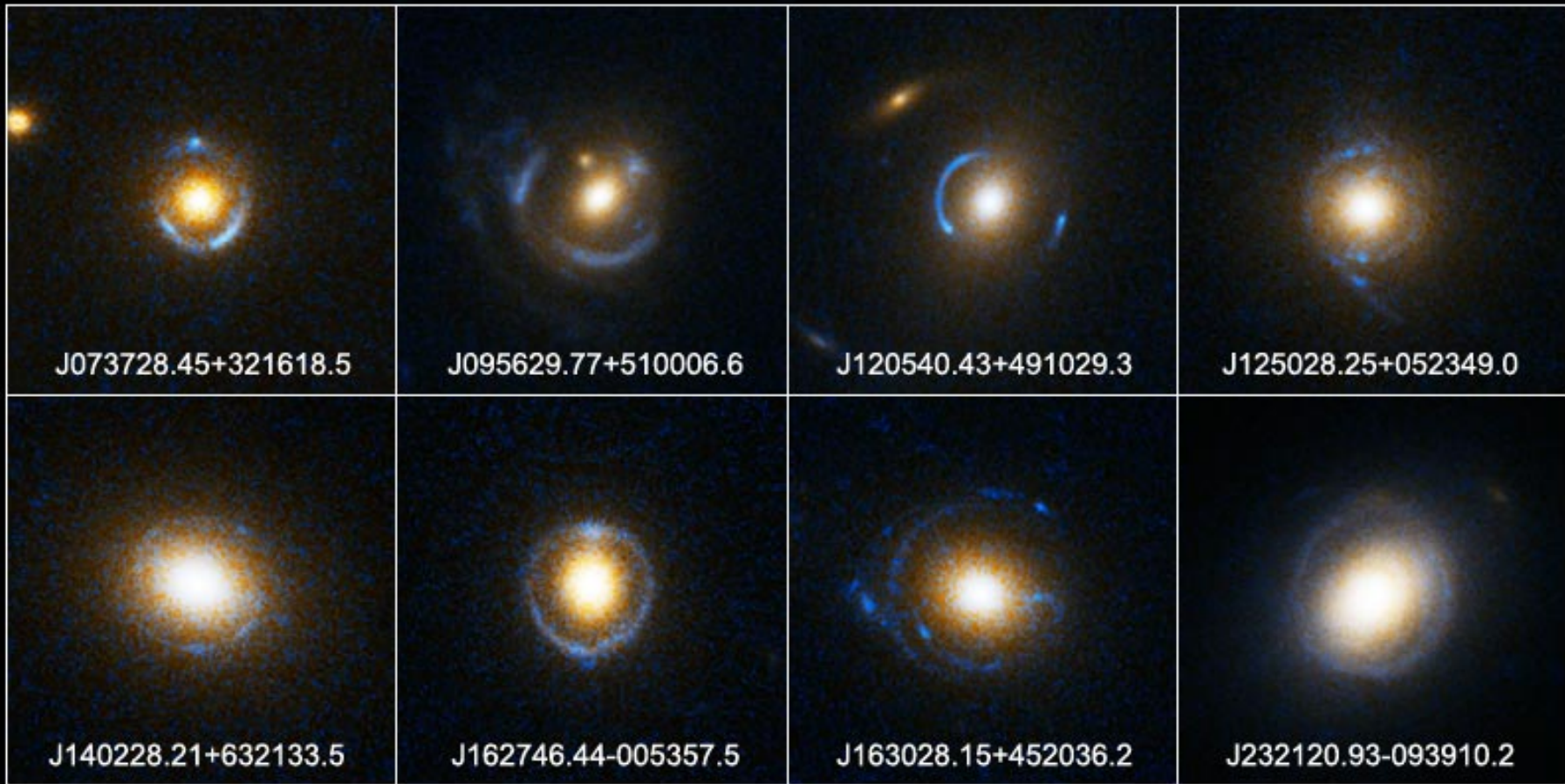


IR Colour Composite of Galaxy Cluster CL2244-02 with Gravitational Arcs
(VLT UT1 + ISAAC)



Einstein Ring Gravitational Lenses

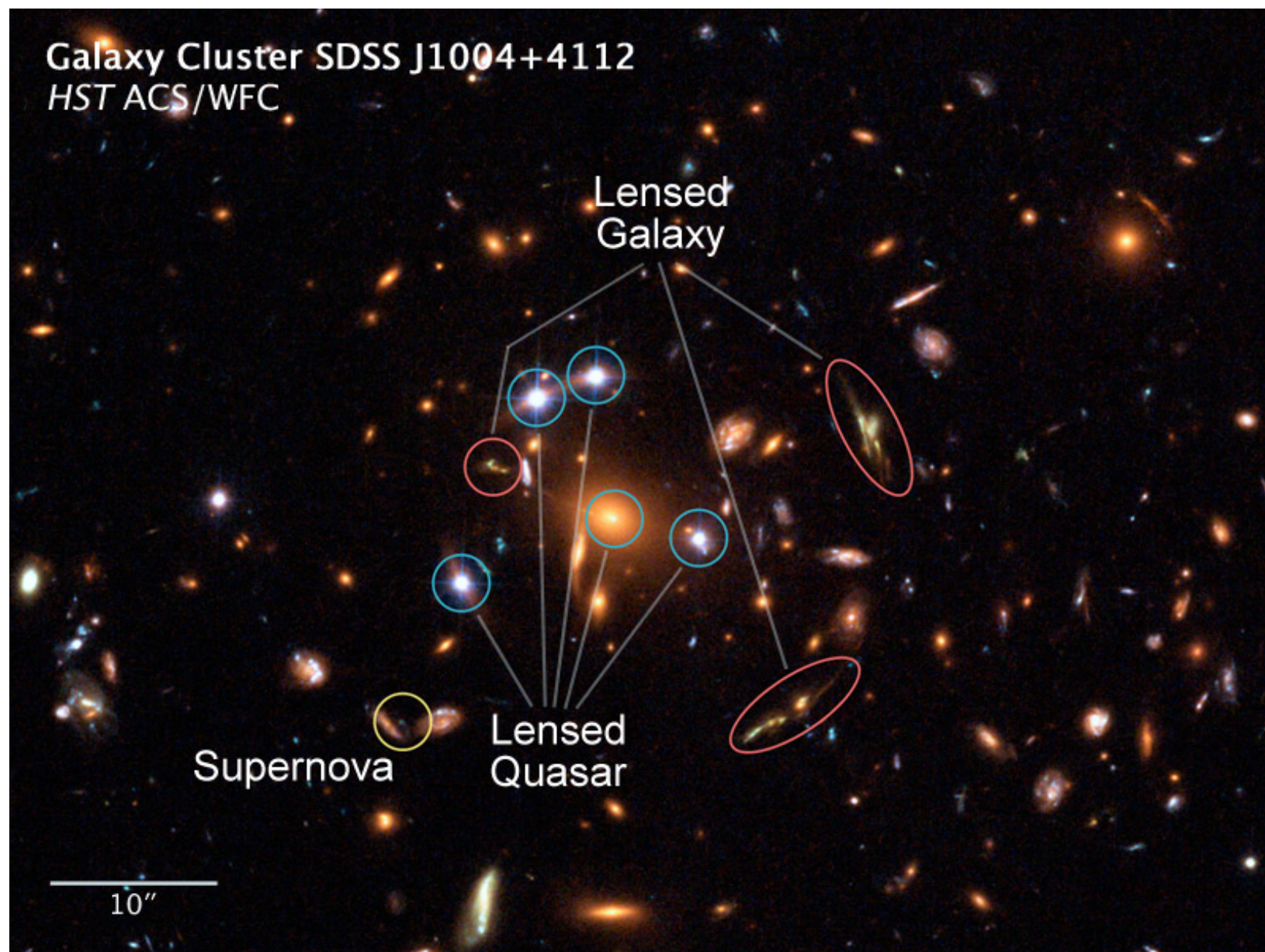
Hubble Space Telescope ■ ACS



NASA, ESA, A. Bolton (Harvard-Smithsonian CfA), and the SLACS Team

STScI-PRC05-32

Galaxy Cluster SDSS J1004+4112
HST ACS/WFC

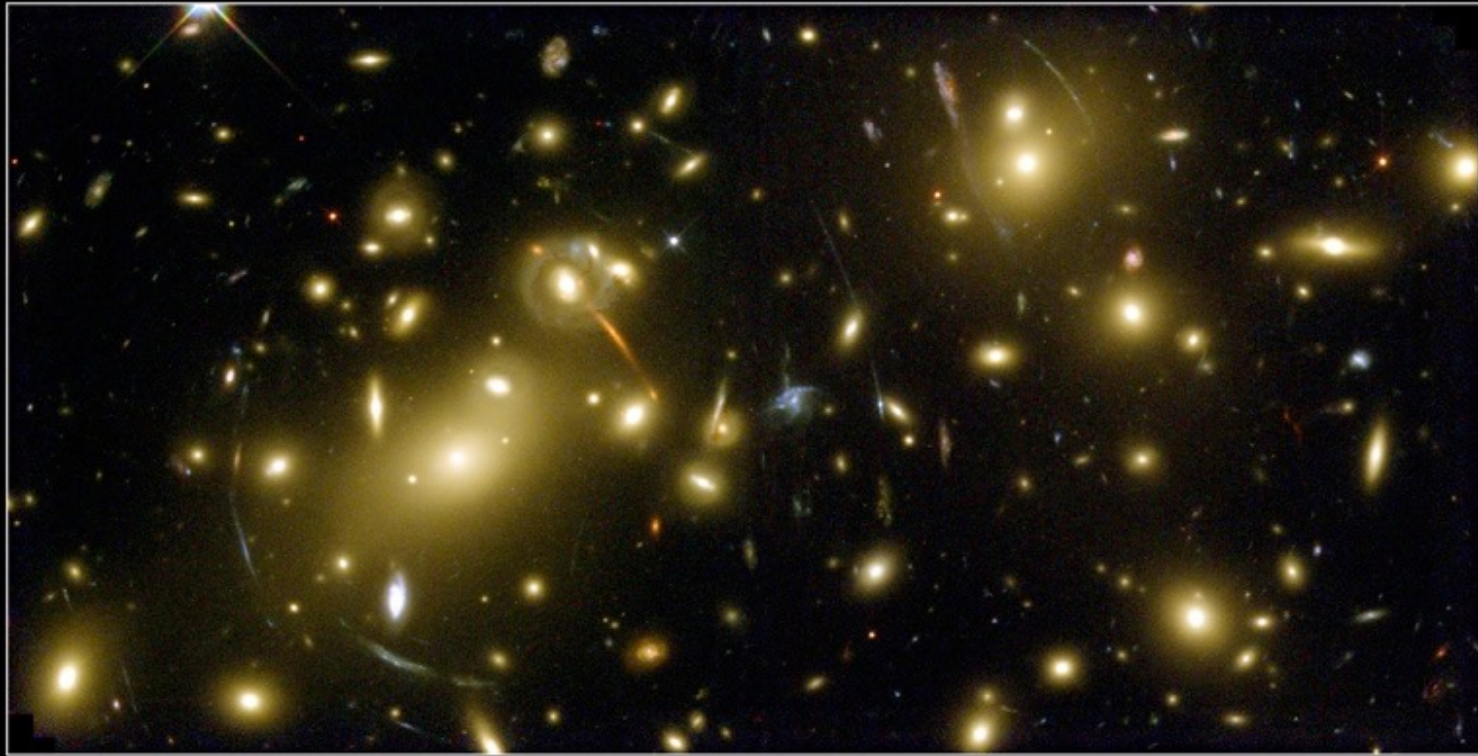


Lensed
Galaxy

Supernova

Lensed
Quasar

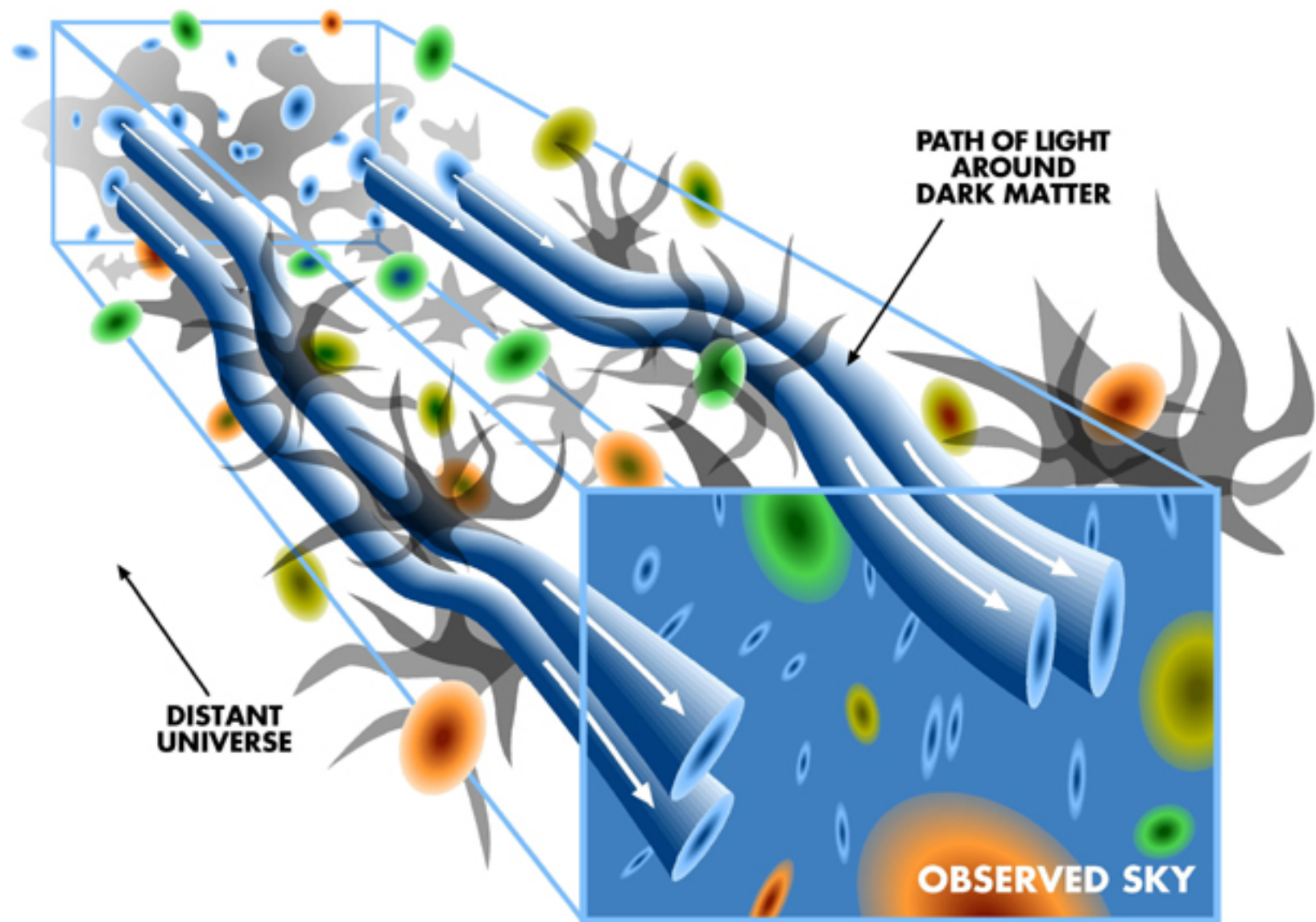
10''



Galaxy Cluster Abell 2218
Hubble Space Telescope • WFPC2

NASA, A. Fruchter and the ERO Team (STScI) • STScI-PRC00-08

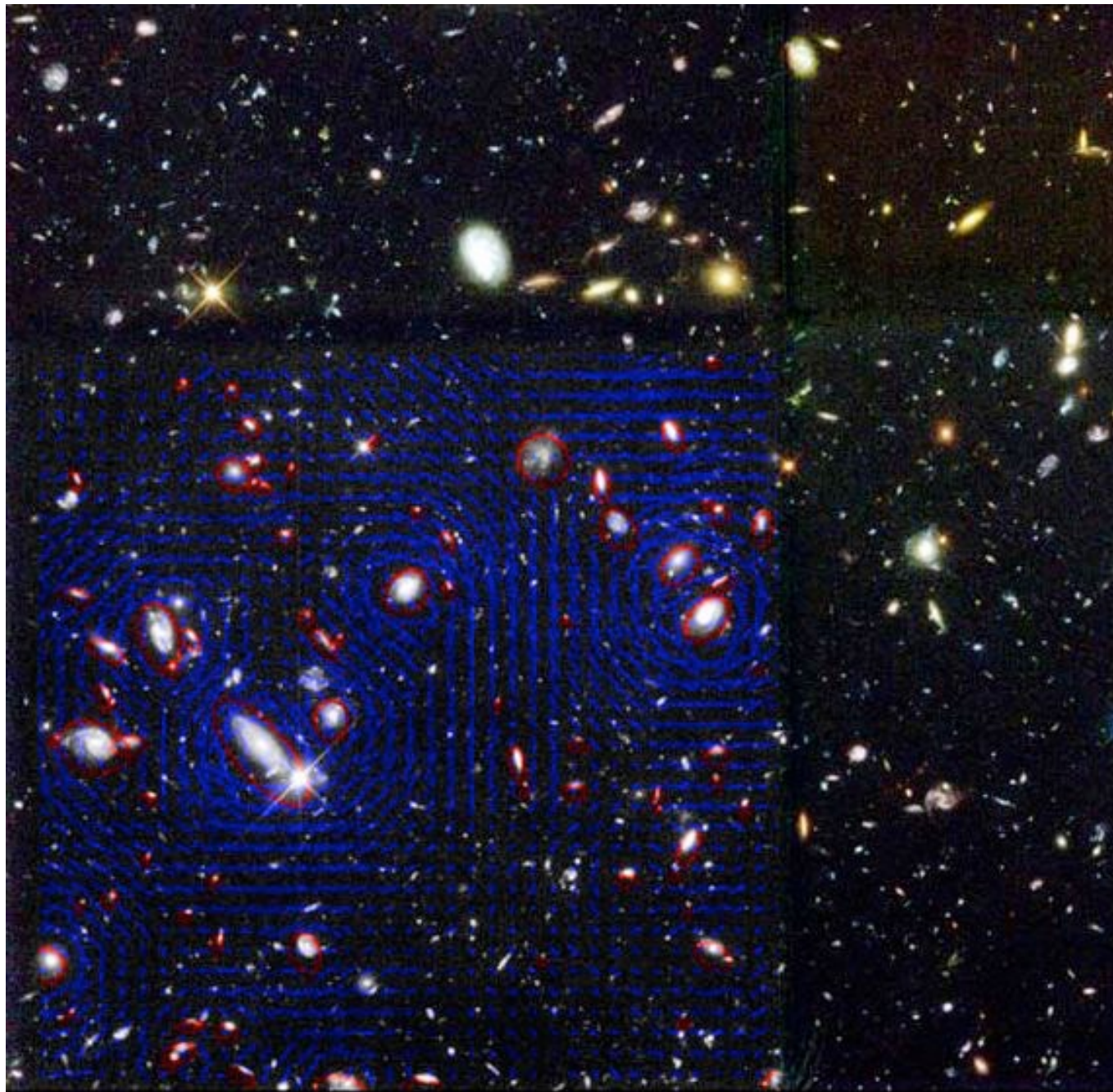


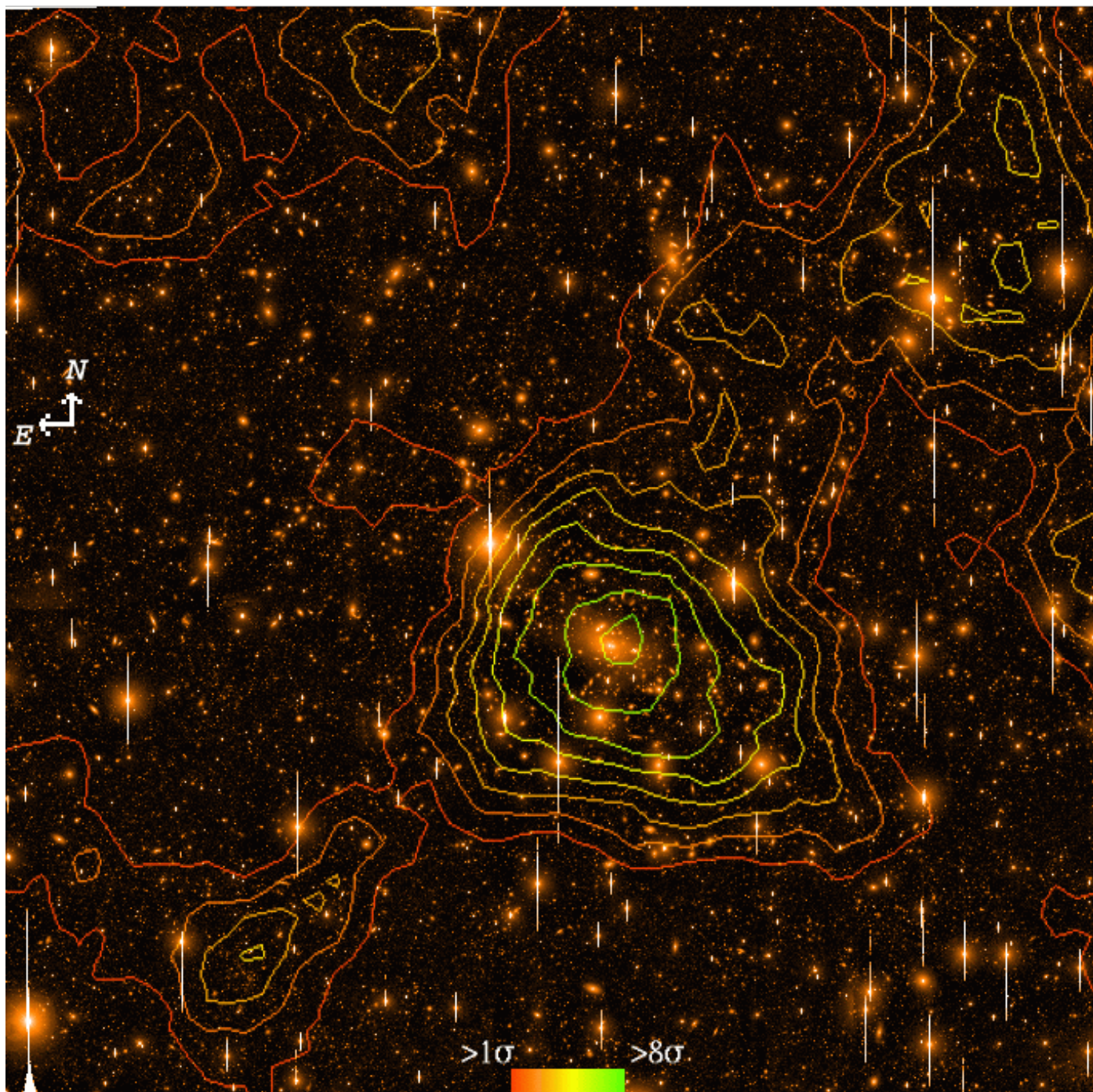


**PATH OF LIGHT
AROUND
DARK MATTER**

**DISTANT
UNIVERSE**

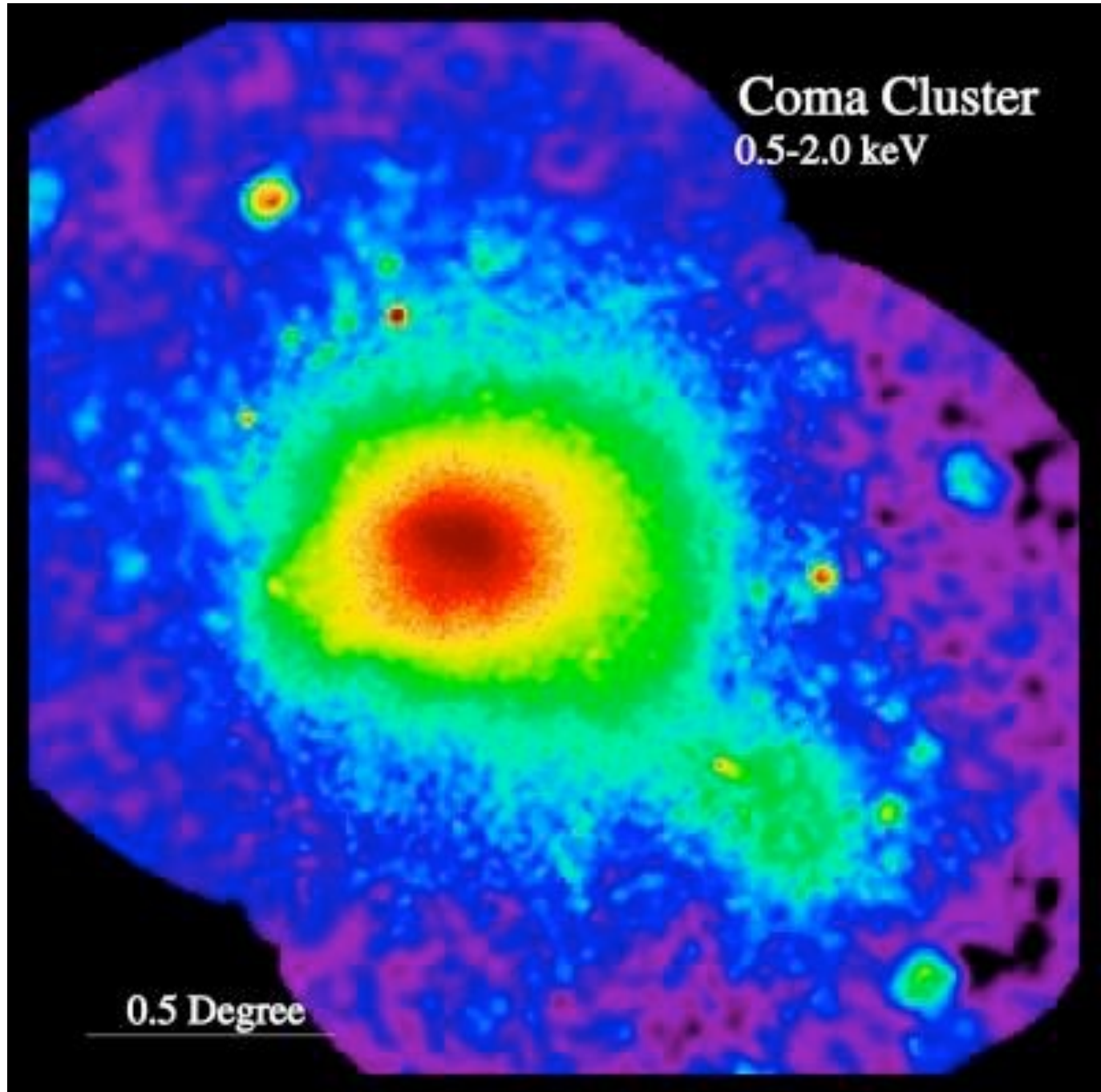
OBSERVED SKY



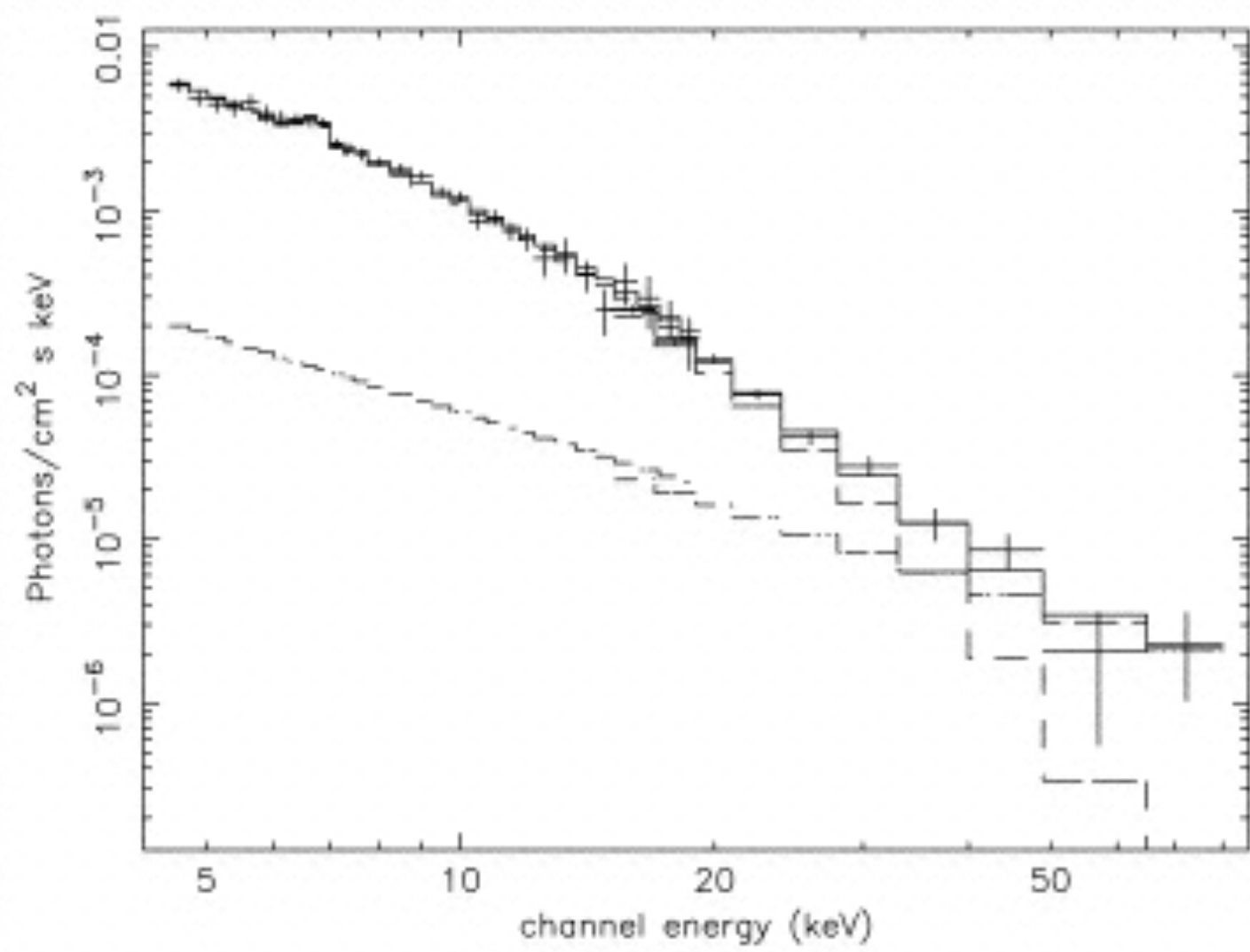


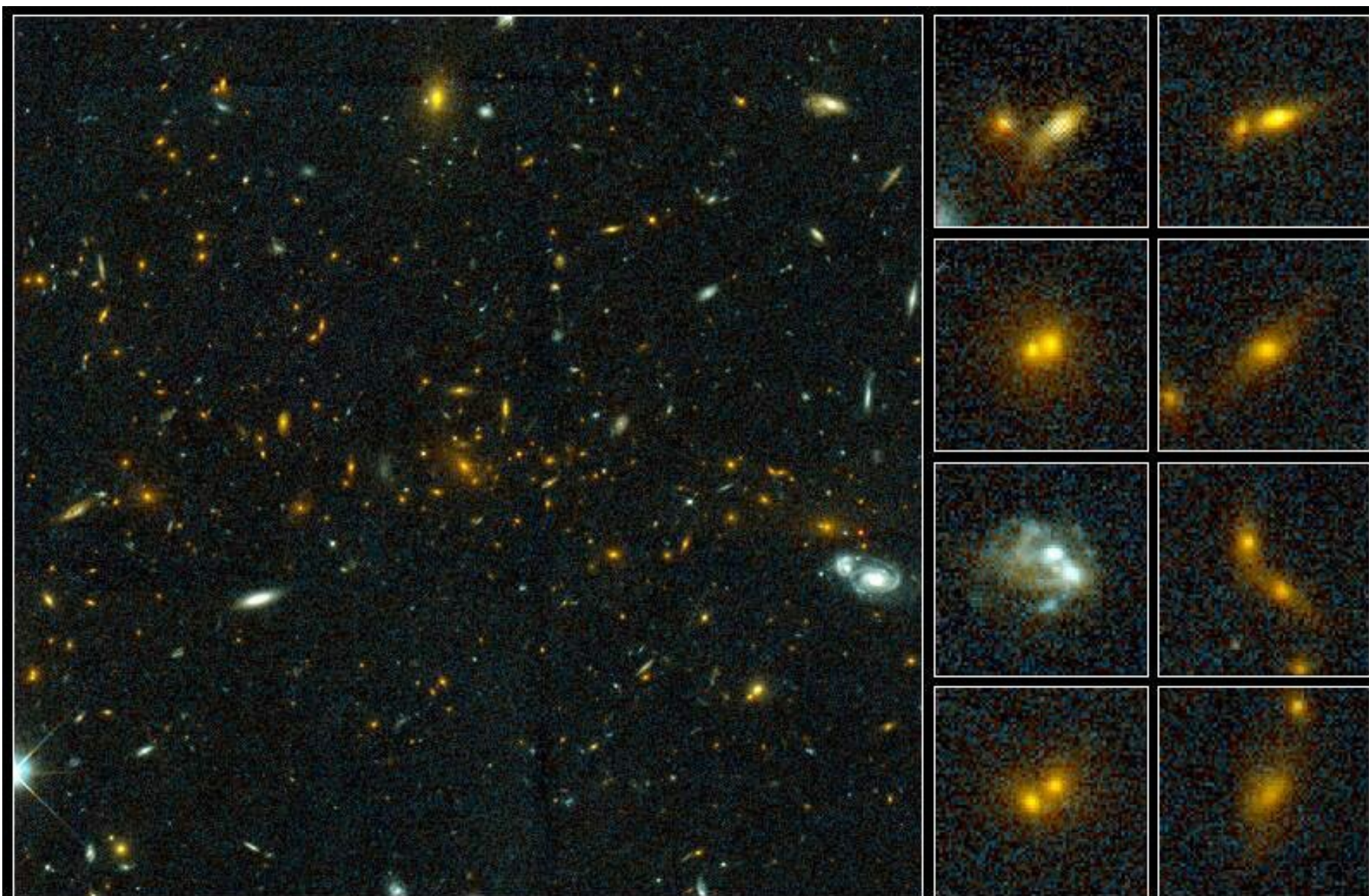


Coma Cluster
0.5-2.0 keV



0.5 Degree



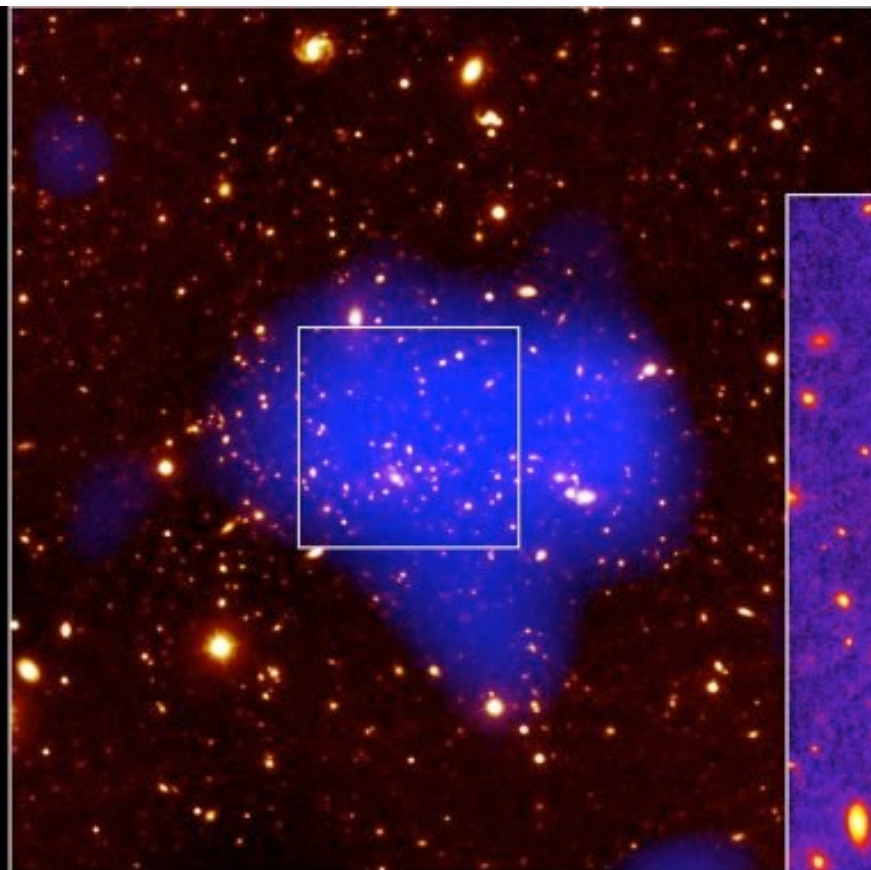


Galaxy Cluster MS1054-03

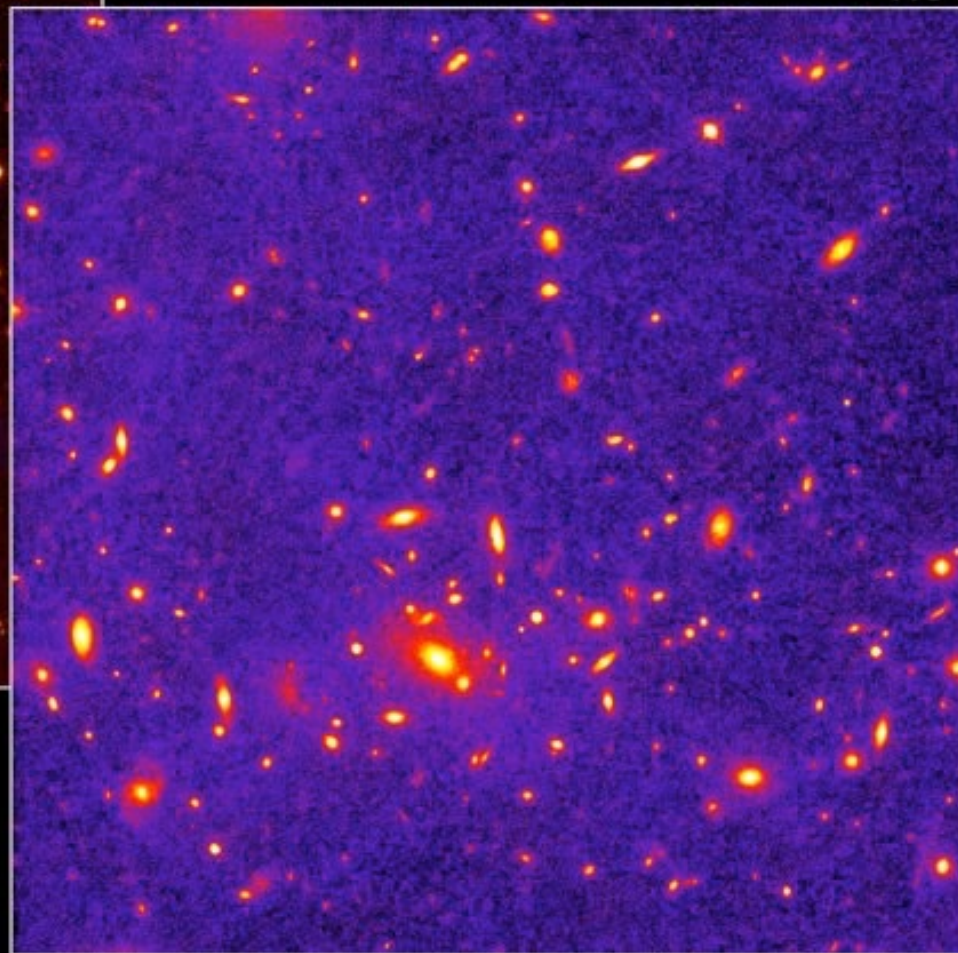
PRC99-28 • STScI OPO • P. van Dokkum (University of Groningen), ESA and NASA

HST • WFPC2

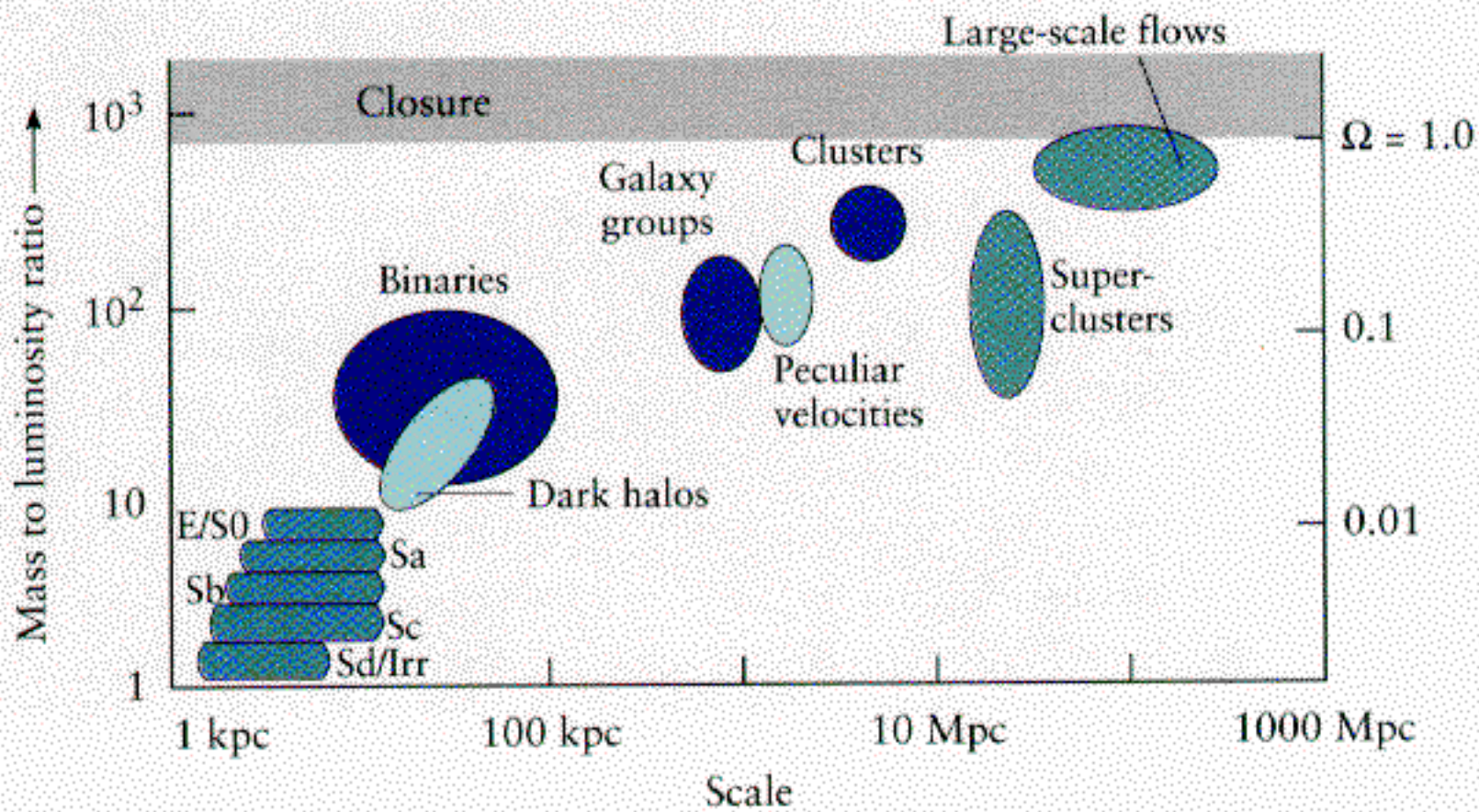
HST



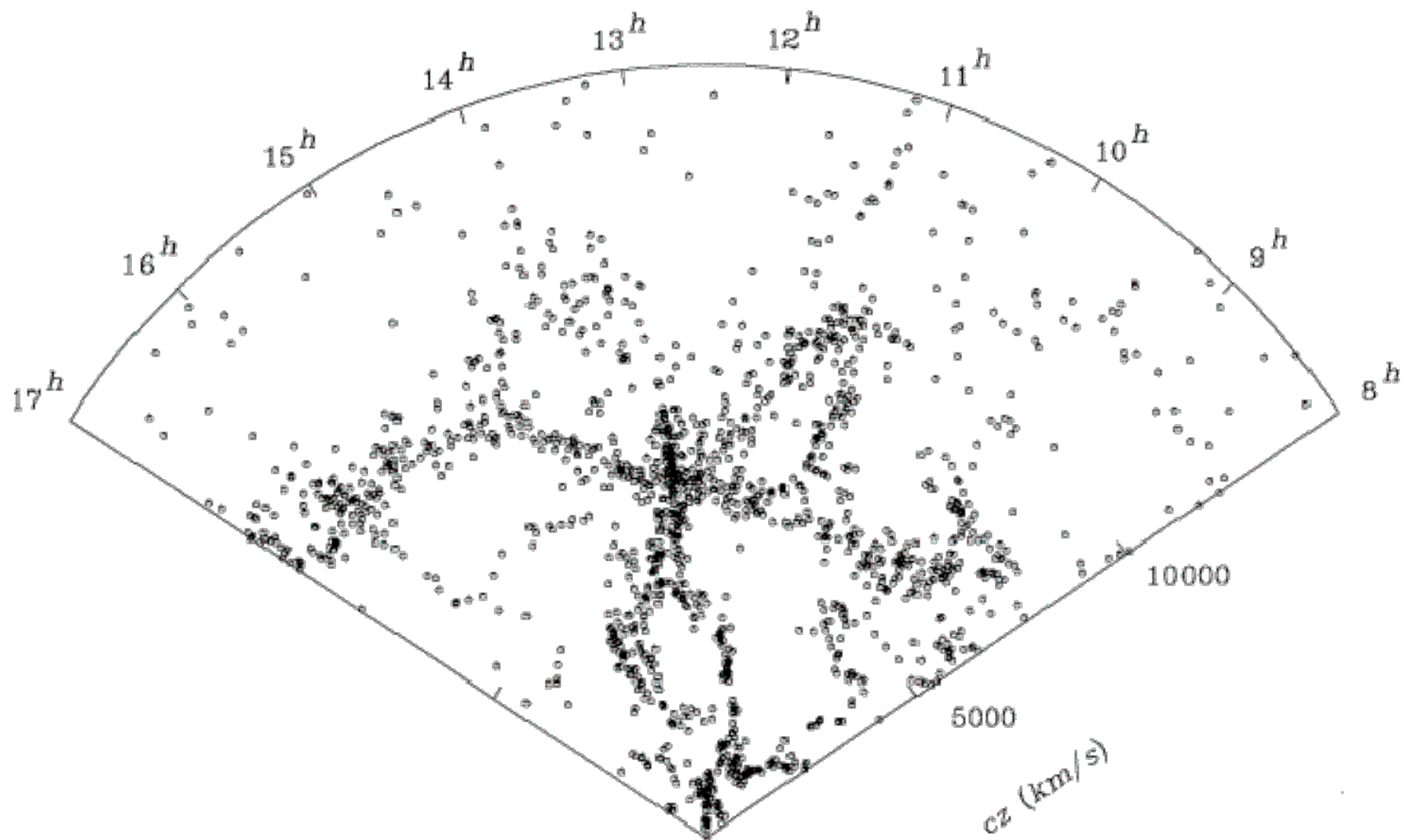
Ground + X-ray

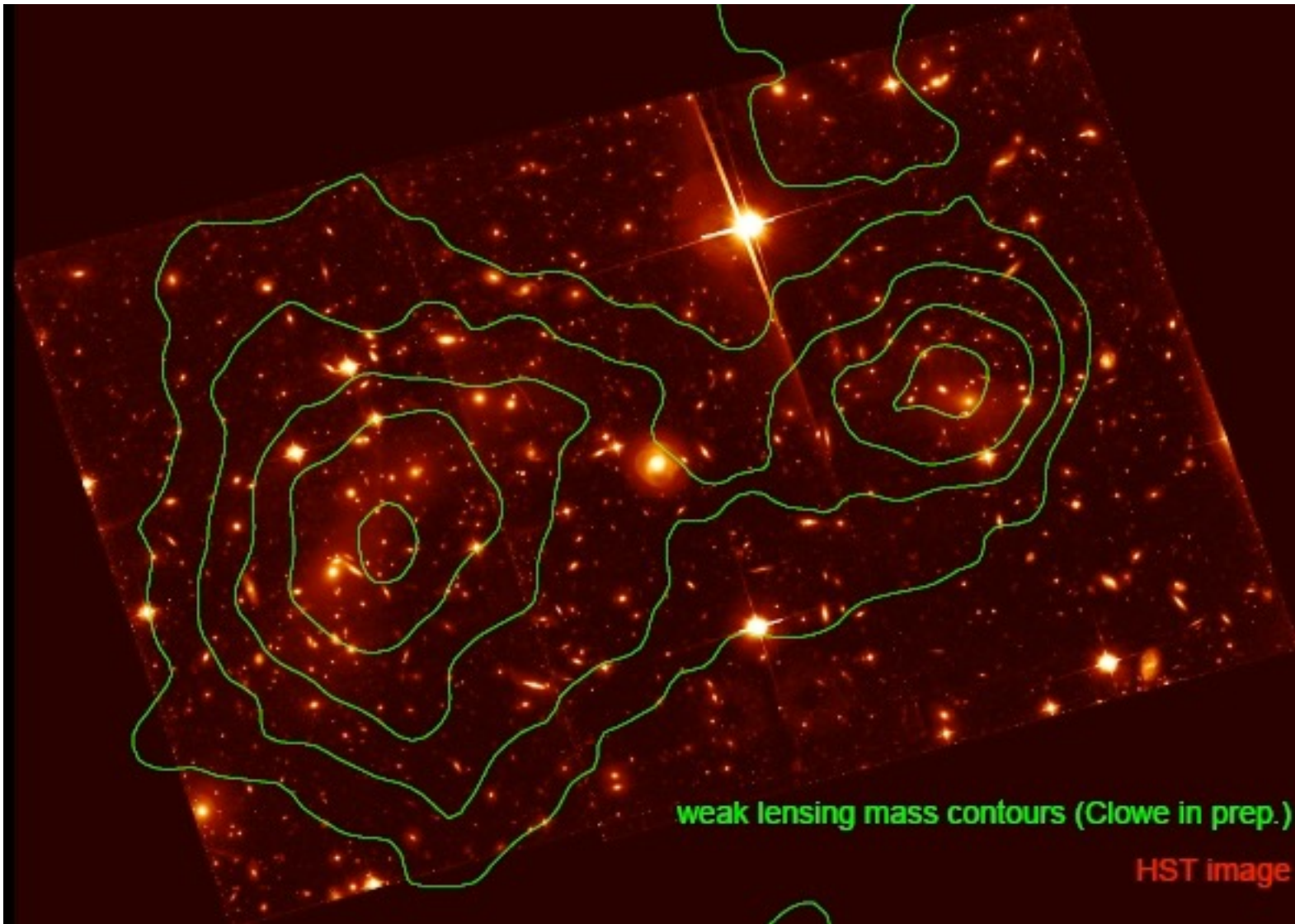


Distant Galaxy Cluster MS1054-0321
Hubble Space Telescope • Wide Field Planetary Camera 2



Non-baryonic		Baryonic	
Axions	(10^{-5} eV)	Snowballs	?
Neutrinos	(~ 10 eV)	Brown dwarfs	($\leq 0.08 M_{\odot}$)
WIMPs	($1-10^3$ GeV)	M-dwarfs	($0.1 M_{\odot}$)
Monopoles	(10^{16} GeV)	White dwarfs	($1 M_{\odot}$)
Planck relics	(10^{19} GeV)	Neutron stars	($2 M_{\odot}$)
Primordial black holes	($> 10^{15}$ g)	Stellar black holes	($\sim 10 M_{\odot}$)
Quark nuggets	($< 10^{20}$ g)	Very Massive Objects	($10^2-10^5 M_{\odot}$)
Shadow matter	?	Super Massive Objects	
Cosmic strings	?	Cold diffuse gas	





1E 0657-56

Chandra 0.5 Msec image

0.5 Mpc

$z=0.3$

